bioRxiv preprint doi: https://doi.org/10.1101/2021.08.04.455154; this version posted August 4, 2021. The copyright holder for this preprint (which was not certified by peer review) is the author/funder. All rights reserved. No reuse allowed without permission.

1 **Opposing roles of p38α-mediated phosphorylation and arginine methylation in driving TDP-**
2 **43 proteinopathy.**
3

4 Mari Aikio[1], Heike J. Wobst[2§], Hana M. Odeh[3], Bo Lim Lee[3], Bradley Class[2], Thomas A.
5 Ollerhead[1], Korrie L. Mack[3,4], Alice F. Ford[3,5], Edward M. Barbieri[3], Ryan R. Cupo[3,6], Lauren E.
6 Drake[3], Nicholas Castello[7], Ashmita Baral[7], John Dunlop[2], Aaron D. Gitler[8], Ashkan Javaherian[7],
7 Steven Finkbeiner[7,9], Dean G. Brown[10§], Stephen J. Moss[1*], Nicholas J. Brandon[1,2*], and James
8 Shorter[3,4,5,6*].
9
10 [1]AstraZeneca-Tufts Laboratory for Basic and Translational Neuroscience, Tufts University, Boston,
11 MA, U.S.A.
12 [2]Neuroscience, BioPharmaceuticals R&D, AstraZeneca, Boston, MA, U.S.A.
13 [3]Department of Biochemistry and Biophysics, [4]Biochemistry and Molecular Biophysics Graduate
14 Group, [5]Neuroscience Graduate Group, [6]Pharmacology Graduate Group, Perelman School of
15 Medicine, University of Pennsylvania, Philadelphia, PA, U.S.A.
16 [7]Center for Systems and Therapeutics, Taube/Koret Center for Neurodegenerative Disease
17 Research, Gladstone Institutes, San Francisco, CA, U.S.A.
18 [8]Department of Genetics, Stanford University School of Medicine, Stanford, CA, U.S.A.
19 [9]Deparments of Neurology and Physiology, University of California, San Francisco, CA, U.S.A.
20 [10]Hit Discovery, Discovery Sciences, BioPharmaceuticals R&D, AstraZeneca, Boston, MA, U.S.A.
21 [§]Current address: Jnana Therapeutics, 6 Tide St., Boston, MA, U.S.A.
22 Running Title: **p38α promotes TDP-43 proteinopathy**
23

24 *To whom correspondence should be addressed: jshorter@pennmedicine.upenn.edu,
25 nick.j.brandon@gmail.com, stephen.moss@tufts.edu
26 Keywords: ALS, TDP-43, p38α, phosphorylation, PRMT1, arginine methylation

bioRxiv preprint doi: https://doi.org/10.1101/2021.08.04.455154; this version posted August 4, 2021. The copyright holder for this preprint (which was not certified by peer review) is the author/funder. All rights reserved. No reuse allowed without permission.

27 **Abstract**

28 Amyotrophic lateral sclerosis (ALS) is a fatal neurodegenerative disorder typically characterized by
29 insoluble inclusions of hyperphosphorylated TDP-43. The mechanisms underlying toxic TDP-43
30 accumulation are not understood. Persistent activation of p38 mitogen-activated protein kinase
31 (MAPK) is implicated in ALS. However, it is unclear how p38 MAPK affects TDP-43 proteinopathy.
32 Here, we demonstrate that inhibition of p38α MAPK reduces pathological TDP-43 phosphorylation,
33 aggregation, cytoplasmic mislocalization, and neurotoxicity. We establish that p38α MAPK
34 phosphorylates TDP-43 at pathological serine 409/410 (S409/S410) and serine 292 (S292), which
35 reduces TDP-43 liquid-liquid phase separation (LLPS) but allows pathological TDP-43 aggregation.
36 Moreover, we show that protein arginine methyltransferase 1 methylates TDP-43 at R293.
37 Importantly, S292 phosphorylation reduces R293 methylation, and R293 methylation reduces
38 S409/S410 phosphorylation. R293 methylation permits TDP-43 LLPS and reduces pathological
39 TDP-43 aggregation. Thus, strategies to reduce p38α-mediated TDP-43 phosphorylation and promote
40 R293 methylation could have therapeutic utility for ALS and related TDP-43 proteinopathies.

41

42

bioRxiv preprint doi: https://doi.org/10.1101/2021.08.04.455154; this version posted August 4, 2021. The copyright holder for this preprint (which was not certified by peer review) is the author/funder. All rights reserved. No reuse allowed without permission.

43 **Introduction**

44 Amyotrophic lateral sclerosis (ALS) is a fatal disorder caused by degeneration of motor neurons
45 (Wobst et al., 2020). While most ALS cases (~90–95%) are considered sporadic with unknown
46 etiology (sALS), ~5–10% of cases are familial in nature (fALS), exhibiting a dominant pattern of
47 inheritance (Rowland and Shneider, 2001; Valdmanis and Rouleau, 2008). ALS is linked to mutations
48 in more than 25 genes, with the C9ORF72 hexanucleotide repeat expansion and mutations in the
49 copper–zinc superoxide dismutase (SOD1) being the most common genetic causes (Nguyen et al.,
50 2018). Although mutations in Transactive Response DNA binding protein 43 kDa (*TARDBP*), the
51 gene encoding TDP-43, are a rare cause of ALS, ~97% of ALS cases and ~50% of patients with
52 frontotemporal dementia (FTD) present with TDP-43 proteinopathy characterized by TDP-43-
53 positive insoluble nuclear and cytoplasmic inclusions in affected neurons (Arai et al., 2006; Guo and
54 Shorter, 2017; Neumann et al., 2006).

55

56 TDP-43 is an essential, highly conserved, ubiquitously expressed, and predominantly nuclear protein
57 with RNA/DNA-binding properties (Portz et al., 2021). It acts as a transcriptional repressor and is
58 implicated in RNA transport and stability, alternative splicing, microRNA biogenesis, and formation
59 of stress granules (SGs) (Alami et al., 2014; Aulas et al., 2012; Buratti and Baralle, 2008; Kawahara
60 and Mieda-Sato, 2012; Khalfallah et al., 2018; Lalmansingh et al., 2011; Li et al., 2018; McDonald
61 et al., 2011; Tollervey et al., 2011). TDP-43 is comprised of an N-terminal domain involved in
62 dimerization and recruitment of other RNA-binding proteins, a bipartite nuclear localization sequence
63 (NLS), two RNA-recognition motifs (RRM1 and RRM2) and a C-terminal glycine-rich, low
64 complexity prion-like domain (PrLD) that mediates protein–protein interactions and formation of
65 membraneless organelles, such as SGs, through liquid–liquid phase separation (LLPS) (Figure 1A)
66 (Ayala et al., 2008; Buratti et al., 2005; Chang et al., 2012; Freibaum et al., 2010; Jiang et al., 2017;
67 Johnson et al., 2009; Li et al., 2018; Molliex et al., 2015; Winton et al., 2008). The majority of ALS-

bioRxiv preprint doi: https://doi.org/10.1101/2021.08.04.455154; this version posted August 4, 2021. The copyright holder for this preprint (which was not certified by peer review) is the author/funder. All rights reserved. No reuse allowed without permission.

68 linked TDP-43 mutations reside in the PrLD, which can enhance aggregation propensity and also
69 indicates that this region of TDP-43 may be prone to pathological protein modifications (Figure 1A)
70 (Harrison and Shorter, 2017; Johnson et al., 2009; Prasad et al., 2019).
71
72 Phosphorylation at serine residues 409/410 (S409/S410) is one of the major pathological markers for
73 TDP-43 inclusions in human brains (Hasegawa et al., 2008; Neumann et al., 2009). In addition to
74 phosphorylation, TDP-43 also undergoes other post-translational modifications (PTMs) in ALS
75 patients and disease-mimicking models, including ubiquitination, generation of C-terminal domain
76 fragments (CTFs), cysteine oxidation, sumoylation, and acetylation (Buratti, 2018). However, the
77 functional and pathological significance of TDP-43 PTMs remains unknown. Thus, a clear
78 understanding of the effects of phosphorylation and other PTMs on solubility, localization, and
79 aggregation propensity of TDP-43 will enable new insights into the mechanisms of ALS
80 pathogenesis.
81
82 The mitogen-activated protein kinase (MAPK) signaling pathway plays a key role in the regulation
83 of cellular differentiation, motility, growth, and survival (Brennan et al., 2021). MAPKs, which
84 include extracellular-signal-regulated kinases (ERK), Jun amino-terminal kinases (JNK) and p38
85 MAPKs, are activated in response to cytokines, growth factors and various stressors including
86 oxidative stress and endoplasmic reticulum stress (Brennan et al., 2021; Cuadrado and Nebreda, 2010;
87 Morrison, 2012). In mammals, p38 MAPKs comprise four isoforms (α, β, γ and δ) (Zarubin and Han,
88 2005). Of these, α and β are expressed in most tissues, including the brain (Yasuda et al., 2011). p38γ
89 is most highly expressed in skeletal muscle, and p38δ in testis, pancreas, kidney and small intestine
90 (Cuenda et al., 1997). Aberrant p38 signaling has been linked to several neurodegenerative diseases,
91 including ALS (Burton et al., 2021). Specifically, p38 MAPK inhibition can reduce motor neuron
92 apoptosis and restore the physiological rate of axonal retrograde transport in SOD1-ALS models

bioRxiv preprint doi: https://doi.org/10.1101/2021.08.04.455154; this version posted August 4, 2021. The copyright holder for this preprint (which was not certified by peer review) is the author/funder. All rights reserved. No reuse allowed without permission.

93 (Dewil et al., 2007; Gibbs et al., 2018; Pickhardt et al., 2019). Furthermore, both genetic and
94 pharmacological inhibition of p38β in a *Drosophila* model of TDP-43 toxicity rescued premature
95 lethality (Zhan et al., 2015).
96
97 In this study, we establish a role for p38α MAPK in promoting TDP-43 proteinopathy. We show that
98 inhibition of p38α MAPK reduces ALS-associated TDP-43 phenotypes, including TDP-43
99 aggregation, S409/S410 phosphorylation, cytoplasmic accumulation, and toxicity. Furthermore, *in*
100 *vitro* kinase assays combined with mass spectrometry revealed that p38α directly phosphorylates
101 TDP-43 at S292 and S409/S410. Subsequent cellular experiments identified S292, a residue
102 previously found to be altered in a genetic risk allele for ALS (S292N) (Xiong et al., 2010; Zou et al.,
103 2012), as an important site in regulating TDP-43 aggregation. We found that phosphorylation at S292
104 induced phosphorylation at S409/S410 and promoted TDP-43 aggregation. Moreover, we found that
105 the residue R293, adjacent to S292, is methylated by protein arginine methyltransferase 1 (PRMT1).
106 Interestingly, loss or gain of function for other PRMTs is implicated in the pathogenesis of
107 neurodegenerative diseases (Ratovitski et al., 2015; Simandi et al., 2018). We found that
108 phosphorylation at S292 inhibited R293 methylation, whereas R293 methylation reduced
109 phosphorylation at S409/S410, suggesting an interplay between phosphorylation at S292 and
110 S409/S410 and methylation at R293. Biochemical studies indicated that S292 and S409/S410
111 phosphorylation reduce TDP-43 LLPS but allow TDP-43 aggregation. By contrast, R293 methylation
112 allows TDP-43 LLPS but reduces TDP-43 aggregation. Taken together, our results reveal additional
113 regulatory mechanisms in TDP-43 homeostasis mediated by p38α and PRMT1. We suggest that
114 strategies aimed at reducing p38α-mediated TDP-43 phosphorylation and promoting R293
115 methylation could have therapeutic utility for ALS and related TDP-43 proteinopathies.
116
117

bioRxiv preprint doi: https://doi.org/10.1101/2021.08.04.455154; this version posted August 4, 2021. The copyright holder for this preprint (which was not certified by peer review) is the author/funder. All rights reserved. No reuse allowed without permission.

118 **Materials and methods**

119 **Plasmids**

120 cDNA sequences were based on the accession number NM_007375.3 for human TARDBP,
121 NM_001315 for human p38α (MAPK14) and NM_001536 for human PRMT1. Plasmids harboring
122 N-terminally myc-tagged wild-type or M337V-mutant TDP-43 sequences were generated as
123 described (Wobst et al., 2017). Plasmids harboring C-terminally Flag-tagged wild-type or mutant
124 human TDP-43 and p38α sequences in the pcDNA3.1+/C-(K)-DYK mammalian expression vector
125 were purchased from Genscript and PRMT1 plasmid was purchased from Origene. TDP-43 bacterial
126 expression vector harboring a C-terminal MBP tag (pJ4M TDP-43-TEV-MBP-6xHis) was purchased
127 from Addgene (Plasmid # 104480). TDP-43 mutations were generated by site-directed mutagenesis
128 using QuikChange (Agilent) and confirmed by DNA sequencing. The presence of the S409:S410E,
129 S409:S410A, S292E, S292N, S292A, S292:S409:S410A, S292:S409:S410E, and R293F mutations
130 in TDP-43, as well as dominant negative (DN) T180A/Y182F (Winzen et al., 1999) and constitutively
131 active (CA) D176A/F327S mutations (Diskin et al., 2004) in p38α were confirmed by DNA
132 sequencing performed by Tufts University Core Facilities (forward sequencing primer 5'-TAA-TAC-
133 GAC-TCA-CTA-TAG-GG-3', reverse sequencing primer 5'-CAG-GAA-ACA-GCT-ATG-AC-3')
134 and Eurofins Genomics (TDP-43 sequencing primer 1 5’-TAA-TAC-GAC-TCA-CTA-TAG-GGG-
135 AAT-TG-3’, sequencing primer 2 5’-CGG-TGA-GGT-GCT-GAT-GGT-CC-3’, sequencing primer
136 3 5’-GGC-TTT-GGC-AAT-TCG-CGT-GG-3’)

137

138

bioRxiv preprint doi: https://doi.org/10.1101/2021.08.04.455154; this version posted August 4, 2021. The copyright holder for this preprint (which was not certified by peer review) is the author/funder. All rights reserved. No reuse allowed without permission.

139 **Synthesis of 6-(2,4-difluorophenoxy)-8-ethyl-2-(2-isopropoxyethylamino)pyrido[2,3-
140 d]pyrimidin-7-one (compound 1)**

141

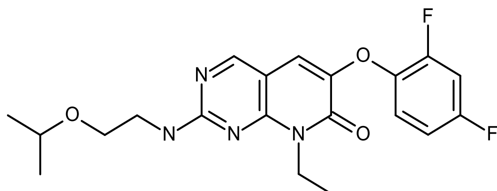

142

143

144 A stirred solution of 2-isopropoxyethan-1-amine (406 mg, 3.93 mmol) was supplemented with 6-
145 (2,4-difluorophenoxy)-8-ethyl-2-(methylsulfonyl)pyrido[2,3-d]pyrimidin-7(8H)-one (300 mg, 0.79
146 mmol) in DMF (3 mL). The resulting solution was stirred at 80 °C for 1 hour in a microwave reactor.
147 The crude product was purified by preparative HPLC (Column: Xselect CSH OBD Column
148 30*150mm 5 µm n;Mobile Phase A:Water (0.1%FA), Mobile Phase B: ACN; Flow rate: 60 mL/min;
149 Gradient: 40% B to 72% B in 8 min; 254/220 nm; Rt: 7.57 min). Fractions containing the desired
150 compound were evaporated to dryness to afford 6-(2,4-difluorophenoxy)-8-ethyl-2-((2-
151 isopropoxyethyl)amino)pyrido[2,3-d]pyrimidin-7(8H)-one (190 mg, 59.7 %) as a white solid. ^{1}H
152 NMR (400 MHz, DMSO-d_6) δ 8.56 (s, 1H), 7.76 (m, 1H), 7.52 - 7.41 (m, 2H), 7.26-7.18 (m, 1H),
153 7.06-7.02 (m, 1H), 4.42-4.32 (m, 2H), 3.65-3.45 (m,5H), 1.28-1.22 (m, 3H), 1.09-1.02 (m, 6H). m/z
154 (ES+), [M+H]+ = 405; TFA, HPLC tR = 1.822 min. The intermediate 6-(2,4-difluorophenoxy)-8-
155 ethyl-2-(methylsulfonyl)pyrido[2,3-d]pyrimidin-7(8H)-one was prepared as described (Goldstein et
156 al., 2011). Compound 1 was tested in a Z'-Lyte kinase assay for p38α (Thermo Fisher) and inhibited
157 p38α activity with an IC_{50} of 25nM.

158

159

bioRxiv preprint doi: https://doi.org/10.1101/2021.08.04.455154; this version posted August 4, 2021. The copyright holder for this preprint (which was not certified by peer review) is the author/funder. All rights reserved. No reuse allowed without permission.

160 **Cell culture, transfections and inhibition of p38α MAPK and methyltransferase activity**

161 SH-SY5Y cells were cultured in minimum essential medium (MEM; Thermo Fisher Scientific)
162 supplemented with L-glutamine, 10% fetal bovine serum and 1% penicillin/streptomycin in a
163 humidified incubator at 37°C and 5% CO_2. For immunocytochemical analysis, cells were grown on
164 glass coverslips coated with 1 mg/mL poly-*L*-lysine (Sigma) in 24-well plates (Cellstar). Cells were
165 transiently transfected using Fugene HD (Promega) following the manufacturer's instructions 24
166 hours after seeding (Fugene HD:DNA ratio 3:1). Total transfection times were 8 hours - 48 hours.
167 For pharmacological inhibition of p38α MAPK, compound 1 (synthesized by AstraZeneca) or equal
168 volume of DMSO vehicle, was added to cells for 24 or 48 hours at a final concentration of 0.1 μM, 1
169 μM or 10 μM. For pharmacological inhibition of arginine methyltransferase activity, adenosine-2′,3′-
170 dialdehyde (AdOx) (Sigma) or equal volume of DMSO vehicle was added to cells for 24 hours at a
171 final concentration of 20 μM.

172

173 **Antibodies**

174 The following antibodies were used for immunocytochemical staining: rabbit N-terminal TDP-43
175 (1:500; 10782-2-AP, Proteintech), mouse anti FLAG-tag (1:500; A00187, GenScript). Anti-rabbit
176 and anti-mouse secondary antibodies coupled to Alexa-488, and Alexa-647 were used for detection
177 (1:1,000; Thermo Fisher Scientific). For western blot analysis, the following antibodies were used:
178 rabbit N-terminal TDP-43 (1:7,000; 10782-2-AP, Proteintech), mouse S409/S410 phospho-TDP-43
179 (1:3,000; CAC-TIP-PTD-M01, Cosmo), rabbit p38 MAPK (1:1,500; 9212S, Cell Signaling
180 Technology), rabbit COX IV (3E11) (1:1,500; 4850, Cell Signaling Technology), mouse Histone H3
181 (96C10) (1:1,500; 3638, Cell Signaling Technology), rabbit Mono-Methyl Arginine (R*GG)
182 (D5A12) (1:1,500; 8711S, Cell Signaling Technology), rabbit Asymmetric Di-Methyl Arginine Motif
183 [adme-R] MultiMab (1:1,500; 13522S, Cell Signaling Technology), rabbit Symmetric Di-Methyl
184 Arginine Motif [sdme-RG] MultiMab (1:1,500; 13222S, Cell Signaling Technology), rabbit PRMT1

bioRxiv preprint doi: https://doi.org/10.1101/2021.08.04.455154; this version posted August 4, 2021. The copyright holder for this preprint (which was not certified by peer review) is the author/funder. All rights reserved. No reuse allowed without permission.

185 (A33) (1:1,500; 2449, Cell Signaling Technology), mouse GAPDH (1:10,000; 60004-1-Ig,
186 Proteintech). Anti-mouse and anti-rabbit horseradish peroxidase-coupled secondary antibodies were
187 purchased from Jackson Immunoresearch (1:10,000).
188

189 **siRNA knockdown of p38α and PRMT1**

190 Small interfering RNAs (siRNA) were obtained from Thermo Fisher Scientific: p38α: s3585 and
191 s3586, PRMT1: s6917, s6919, Negative control: 4390846, 4390843. Reverse transfection was
192 performed with Lipofectamine RNAiMAX-reagent (Invitrogen) following the manufacturer's
193 instructions. In brief, 25 pmol of siRNA were mixed with 5 µL of Lipofectamine RNAiMAX in 500
194 µL of Opti-MEM (Invitrogen) in a 6-well plate. The mixture was incubated for 20 min at room
195 temperature and 3-3.5 x 10^5 cells were added to mixture. Total knockdown times were 8 - 72 hours.
196

197 **Sequential extraction of insoluble protein aggregates**

198 Extraction of insoluble proteins was performed as previously described (Wobst et al., 2017). Briefly,
199 transfected cells were lysed in 300 µL radio-immunoprecipitation assay (RIPA) buffer [50 mM Tris-
200 HCl, 150 mM NaCl, 1% NP-40, 0.5% sodium deoxycholate, and 0.1% SDS] (Boston bioproducts)
201 supplemented with 2 mM EDTA, protease inhibitors (cOmplete, Roche), and phosphatase inhibitors
202 (PhosStop, Roche). Lysates were sonicated 2 x 15 s with 20% maximum amplitude and centrifuged
203 for 30 min at 100,000 × *g* and 4°C. The supernatant was collected as the RIPA-soluble fraction. The
204 pellet was washed in RIPA buffer and centrifuged as above. The supernatant was discarded and the
205 urea-soluble fraction was generated by resuspending the pellet in 100 µL urea buffer [7 M urea, 2 M
206 thiourea, 30 mM Tris pH 8.5, 4% 3-[(3-Cholamidopropyl) dimethylammonio]-1-propanesulfonate
207 (CHAPS, Sigma)], and sonicating the samples as above followed by centrifugation at room
208 temperature for 30 min at 100,000 × g. The supernatant was collected as the urea-soluble fraction.
209

bioRxiv preprint doi: https://doi.org/10.1101/2021.08.04.455154; this version posted August 4, 2021. The copyright holder for this preprint (which was not certified by peer review) is the author/funder. All rights reserved. No reuse allowed without permission.

210 **Immunoblotting**

211 Cell extracts or RIPA and urea fractions obtained from sequential extractions were diluted with
212 NuPAGE sample buffer. Proteins were separated on 4-12% NuPAGE Bis-Tris gels (Thermo Fisher
213 Scientific) under denaturing conditions and transferred onto polyvinylidene difluoride (PVDF)
214 membranes (Millipore). All blocking and antibody incubation steps were performed either in 5% milk
215 in Tris-buffered saline (TBS) [25 mM Tris, 3 mM KCl, 140 mM NaCl, pH 7.4] supplemented with
216 0.05% Tween-20 (TBS-T) (Thermo Fisher Scientific) or in 5% bovine serum albumin (BSA) in TBS-
217 T. Western blots were developed with enhanced chemiluminescent substrates (ECL). Digital images
218 were acquired with a ChemiDoc MP imaging system (BioRad). Where necessary, blots were stripped
219 with stripping buffer for 15 min (Restore, Thermo Fisher Scientific) and re-probed with loading
220 control antibodies.

221

222 **Lactate Dehydrogenase (LDH) assay to monitor cell death**

223 NSC-34 cells were cultured in Dulbecco's modified Eagle's medium (DMEM, Thermo Fisher
224 Scientific), supplemented with 10% fetal bovine serum and 1% penicillin/streptomycin in a
225 humidified incubator at 37°C and 5% CO_2. Cells grown on 96-well plates coated with poly-*L*-lysine
226 (BioCoat multiwell plates, Corning) were transiently transfected using Lipofectamine 3000 (Thermo
227 Fisher Scientific) following the manufacturer's instructions 24 h after seeding (Lipofectamine
228 3000:DNA ratio 3:1). Cells were treated with DMSO or p38α MAPK inhibitor (compound 1) at final
229 concentrations of 1 or 10 μM for 4 hours post-transfection. LDH activity was measured from 50 μL
230 of conditioned medium using LDH assay kit (Life Technologies) following the manufacturer's
231 instructions.

232

233

bioRxiv preprint doi: https://doi.org/10.1101/2021.08.04.455154; this version posted August 4, 2021. The copyright holder for this preprint (which was not certified by peer review) is the author/funder. All rights reserved. No reuse allowed without permission.

234 **Longitudinal imaging and neuronal survival analysis**

235 Primary cortical neurons from E17 mouse embryos were cultured in 384-well plates. Neurons were
236 co-transfected with plasmids expressing the fluorescent marker mApple and TDP-43^{M337V}-EGFP.
237 Neurons were treated with p38α inhibitor, VX-745 (synthesized by AstraZeneca), at 0.3, 1, 3, or 9
238 μM, and imaged daily for 7 days on a custom-built highthroughput robotic microscopy system
239 (Arrasate and Finkbeiner, 2005; Barmada et al., 2010). Images were montaged and neurons were
240 segemented and tracked using custom-built algorithms. Cox proportional hazard analysis was used to
241 determine hazard ratios. DMSO was used as a control.

242

243 **Cytoplasmic and nuclear protein extraction**

244 Cytoplasmic and nuclear protein extraction was performed using a commercial subcellular protein
245 fractionation kit (Thermo Fisher Scientific). Briefly, ~80% confluent SH-SY5Y cells plated in a 100
246 -mm dish were transfected as indicated for 24 hours. Cells were trypsinized and rinsed with cold
247 phosphate-buffered saline (PBS), and cell suspensions were transferred to pre-chilled 1.5 mL
248 microcentrifuge tubes. Cells were lysed in cytoplasmic extraction buffer at 4°C for 10 minutes with
249 gentle mixing. After centrifugation at 500 x g at 4 °C for 5 min, the supernatant was collected and
250 stored as the cytoplasmic fraction. After addition of membrane extraction buffer to the pellet, the tube
251 was vortexed vigorously for 5 s and incubated at 4°C for 10 minutes with gentle mixing. After
252 centrifugation at 3,000 x g at 4 °C for 5 min, the supernatant was collected and stored as the membrane
253 fraction. The pellet was resuspended in nuclear extraction buffer followed by vigorous vortexing for
254 15 s and incubation at 4°C for 30 minutes with gentle mixing. After centrifugation at 5,000 x g at
255 4 °C for 5 min, the supernatant was collected and stored as the soluble nuclear fraction. The pellet
256 was resuspended in chromatin-bound extraction buffer followed by vigorous vortexing for 15 s and
257 incubation at room temperature for 15 s. The vortexing and incubation steps were repeated twice.
258 After centrifugation at 16,000 x g at 4 °C for 5 min, the supernatant was collected and stored as the

bioRxiv preprint doi: https://doi.org/10.1101/2021.08.04.455154; this version posted August 4, 2021. The copyright holder for this preprint (which was not certified by peer review) is the author/funder. All rights reserved. No reuse allowed without permission.

259 chromatin-bound nuclear fraction. Bicinchoninic acid (BCA) assay was used to measure protein
260 concentrations.
261
262 **Immunocytochemistry**
263 Cells grown on poly-*L*-lysine-coated glass coverslips were washed in PBS and fixed in 4%
264 paraformaldehyde (in PBS) for 15 min followed by permeabilization in 0.25% Triton-X (in PBS) for
265 10 min. Cells were blocked with 10% normal goat serum (in PBS, Abcam) for 1 h at room temperature
266 and incubated overnight at 4°C in primary antibody diluted in blocking solution. The next day, cells
267 were washed with PBS and incubated for 1 h in secondary antibody diluted in blocking solution.
268 Coverslips were mounted with Prolong Gold Antifade Mountant with DAPI (Thermo Fisher
269 Scientific). Image acquisition was performed using a Nikon A1 confocal/Eclipse Ti inverted
270 microscope system and NIS Elements software (Nikon).
271
272 **Protein kinase assays with recombinant proteins**
273 5 μL of 10x kinase assay buffer [25 mM Tris (pH 7.5), 5 mM β-glycerophosphate, 2 mM DTT, 0.1
274 mM Na_2VO_4, 10 mM $MgCl_2$] (Cell Signaling Technology), 200 μM ATP (Cell Signaling
275 Technology), 750 ng of recombinant human TDP-43 protein (Proteintech) and 300 ng of recombinant
276 active p38α kinase (SignalChem) were mixed in pre-chilled 1.5 mL tubes. Reactions were made up
277 to a total volume of 50 μL with ddH_2O. Samples were mixed by flicking the tubes followed by brief
278 centrifugation at 4°C and incubation at 30°C for 30 min. When indicated, kinase reactions were
279 treated with 10 μM the p38α inhibitor compound 1. Reactions were stopped by adding 18 μL of 4×
280 NuPAGE sample buffer and boiling samples at 95°C for 5 minutes. Samples were subjected to
281 immunoblotting or Coomassie staining followed by phosphorylation analysis by LC-MS/MS.
282
283

bioRxiv preprint doi: https://doi.org/10.1101/2021.08.04.455154; this version posted August 4, 2021. The copyright holder for this preprint (which was not certified by peer review) is the author/funder. All rights reserved. No reuse allowed without permission.

284 **Phosphorylation analysis by LC-MS/MS**

285 *In vitro* kinase reactions were separated on 4-12% NuPAGE Bis-Tris gels (Thermo Fisher Scientific)
286 and gel bands were visualized with SimplyBlue™ SafeStain (Thermo Fisher Scientific). Gel bands
287 were excised and cut into ~1 mm^3 pieces. The samples were reduced with 1 mM dithiothreitol (DTT)
288 for 30 minutes at 60ºC and then alkylated with 5 mM iodoacetamide for 15 minutes at room
289 temperature. Gel pieces were then subjected to a modified in-gel trypsin digestion procedure
290 (Shevchenko et al., 1996). Briefly, gel pieces were washed and dehydrated with acetonitrile for 10
291 min followed by removal of acetonitrile. Pieces were then completely dried using a speed-vac. Gel
292 pieces were rehydrated in 50 mM ammonium bicarbonate solution containing 12.5 ng/µL modified
293 sequencing-grade trypsin (Promega) at 4ºC before incubation overnight at 37°C. Peptides were later
294 extracted by removing the ammonium bicarbonate solution, followed by one wash with a solution
295 containing 50% acetonitrile and 1% formic acid. The extracts were then dried in a speed-vac for 1
296 hour and stored at 4ºC until analysis. On the day of analysis, samples were reconstituted in 5 - 10 µL
297 of High Performance Liquid Chromatography (HPLC) solvent A (2.5% acetonitrile, 0.1% formic
298 acid). A nano-scale reverse-phase HPLC capillary column was created by packing 2.6 µm C18
299 spherical silica beads into a fused silica capillary (100 µm inner diameter, ~30 cm length) with a
300 flame-drawn tip (Peng and Gygi, 2001). After equilibrating the column, each sample was loaded onto
301 the column via a Famos auto sampler (LC Packings). A gradient was formed, and peptides were
302 eluted with increasing concentrations of solvent B (97.5% acetonitrile, 0.1% formic acid). As each
303 peptide was eluted it was subjected to electrospray ionization before entering an LTQ Orbitrap Velos
304 Pro ion-trap mass spectrometer (Thermo Fisher Scientific). Eluting peptides were detected, isolated,
305 and fragmented to produce a tandem mass spectrum of specific fragment ions for each peptide.
306 Peptide sequences were determined by matching protein or translated nucleotide databases with the
307 acquired fragmentation pattern using the software program Sequest (Thermo Finnigan) (Eng et al.,
308 1994). The modification of 79.9663 mass units to serine, threonine, and tyrosine was included in the

bioRxiv preprint doi: https://doi.org/10.1101/2021.08.04.455154; this version posted August 4, 2021. The copyright holder for this preprint (which was not certified by peer review) is the author/funder. All rights reserved. No reuse allowed without permission.

309 database searches to determine phosphopeptides. Phosphorylation assignments were determined
310 using the Ascore algorithm (Beausoleil et al., 2006). All databases include a reversed version of all
311 sequences and the data was filtered to 1-2% peptide false discovery rate.
312

313 **Co-immunoprecipitation (Co-IP)**

314 Approximately 80% confluent SH-SY5Y cells plated in 6-well plates or 100-mm dishes were
315 transfected as indicated. Cells were rinsed with cold PBS, and then lysed in cold lysis buffer [20 mM
316 Tris-HCl (pH 7.5), 150 mM NaCl, 1 mM Na_2EDTA, 1 mM EGTA, 1% Triton, 2.5 mM sodium
317 pyrophosphate, 1 mM beta-glycerophosphate, 1 mM Na_3VO_4, 1 µg/mL leupeptin] (Cell Signaling
318 Technology), supplemented with protease inhibitors (cOmplete, Roche). Cells were incubated on ice
319 for 5 minutes, collected in pre-chilled 1.5 mL tubes, sonicated briefly and cleared by centrifugation
320 (14,000 x g at 4°C for 10 min). Lysate aliquots were stored as the input samples. Cell lysates were
321 either incubated with Anti-FLAG® M2 Magnetic Beads (Millipore Sigma) overnight with continuous
322 rotation at 4°C, or were subjected to pre-cleaning with protein A Dynabeads (Thermo Fisher
323 Scientific) for 1 hour at 4°C followed by incubation with indicated primary antibodies overnight with
324 continuous rotation at 4°C. Protein A Dynabeads were then added to pre-cleared antibody-containing
325 samples, and the incubation was continued for an additional 2 hours at room temperature. Beads with
326 immunoprecipitated proteins were washed 5x with either TBS [50 mM Tris HCl, 150 mM NaCl, pH
327 7.4] (Anti-FLAG® M2 Magnetic Beads) or lysis buffer (Protein A Dynabeads). Immunoprecipitated
328 proteins were eluted with 2x NuPAGE sample buffer by boiling for 3 min. Both input samples and
329 immunoprecipitated proteins were analyzed by immunoblotting.
330

331 **Purification of recombinant TDP-43-MBP**

332 Wild-type TDP-43-MBP-6xHis and TDP-43 mutants S292E, S409:S410E, S292:S409:S410E, and
333 R293F were expressed and purified as previously described (Wang et al., 2018). Briefly, TDP-43

bioRxiv preprint doi: https://doi.org/10.1101/2021.08.04.455154; this version posted August 4, 2021. The copyright holder for this preprint (which was not certified by peer review) is the author/funder. All rights reserved. No reuse allowed without permission.

334 variants were expressed in *E. coli* BL21-CodonPlus (DE3)-RIL cells (Agilent). Cell cultures were
335 grown to an OD_{600} of ~0.5-0.7 and then cooled down to 16°C. Protein expression was induced with
336 1 mM IPTG overnight. Cells were harvested and resuspended in purification buffer (20 mM Tris-
337 HCl, pH 8.0, 1 M NaCl, 10 mM imidazole, 10% (v/v) glycerol, 2 mM β-mercaptoethanol
338 supplemented with cOmplete EDTA-free protease inhibitor cocktail) and lysed using 1 mg/mL
339 lysozyme and sonication. Proteins were purified using Ni-NTA agarose (Qiagen) and eluted using
340 300 mM imidazole in purification buffer. Proteins were then further purified over amylose resin
341 (NEB) and eluted with elution buffer (20 mM Tris-HCl, pH 8.0, 1 M NaCl, 10 mM imidazole, 10
342 mM maltose, 10% (v/v) glycerol, and 1 mM DTT). Purified proteins were concentrated, flash frozen
343 and stored at -80°C.
344
345 ***In vitro* TDP-43 aggregation assay**
346 Purified recombinant TDP-43-MBP-6xHis wild-type and TDP-43 mutants were first thawed and
347 buffer exchanged into 20 mM HEPES-NaOH, pH 7.4, 150 mM NaCl and 1mM DTT using Micro
348 Bio-Spin™ P-6 Gel Columns (Bio-Rad). Protein concentration was determined by NanoDrop, and
349 the final concentration of TDP-43 was then adjusted to 5 μM in the same buffer. To measure
350 aggregation kinetics, aggregation was initiated by cleavage of the MBP-6xHis tag using 1 μg/mL
351 TEV protease (Cupo and Shorter, 2020) at t = 0, and turbidity was measured over 16 h at an
352 absorbance of 395 nm using a TECAN M1000 plate reader. Values were normalized to wild-type
353 TDP-43 + TEV protease to determine the extent of aggregation of TDP-43 mutants.
354
355 ***In vitro* TDP-43 LLPS assay**
356 Purified recombinant TDP-43-MBP-6xHis wild-type and TDP-43 mutants were thawed and buffer
357 exchanged as described above for the aggregation assay. Protein concentration was determined by
358 NanoDrop, and reactions were prepared in phase separation buffer (20 mM HEPES-NaOH, pH 7.4,

bioRxiv preprint doi: https://doi.org/10.1101/2021.08.04.455154; this version posted August 4, 2021. The copyright holder for this preprint (which was not certified by peer review) is the author/funder. All rights reserved. No reuse allowed without permission.

359 150 mM NaCl, 1mM DTT, 100 mg/mL dextran from *Leuconostoc spp.* (Sigma)). Protein was always
360 added last to each phase separation reaction, at a final concentration of 10 µM. Reactions were
361 incubated for 30 min at room temperature, and then 7.5 µL of each reaction was mounted onto a glass
362 slide and imaged by differential interference contrast (DIC) microscopy.
363

364 **Droplet image analysis**

365 DIC images of TDP-43 wild-type and its variants were analyzed using custom-written code in
366 MATLAB. Each image was first converted into grayscale for processing. Then, Roberts gradient
367 was used to filter out the noise. The pixel weight for each pixel in the image was determined based
368 on the grayscale intensity differences before segmenting the images. The threshold for image
369 segmentation was adjusted manually to ensure complete and accurate conversion to logical array.
370 Droplets in the images were identified using circle Hough transform. The sensitivity was toggled
371 either to detect missed droplets or to reduce the number of false positives. The detected circles were
372 visualized on the original images. Various quantitative parameters, including the average area, total
373 area, number of droplets and the lists of areas, were given as outputs to the code and were analyzed
374 further through GraphPad Prism. The accuracy of the circule Hough transform was limited for
375 droplets that were smaller than 5 pixels, where 10.8 pixels are equivalent to 1µm.

376

377 **Quantification of immunocytochemistry and western blots, and statistical analysis**

378 Western blot band densities and immunocytochemical staining were quantified with ImageJ-Win64
379 software. For statistical analysis, we used GraphPad Prism 7 and 8, and used unpaired t-test or one-
380 way ANOVA followed by Sidak's or Dunnett's multiple comparison test, as indicated for each
381 experiment. All assays were repeated at least three times. A *p*-value less than 0.05 was considered
382 statistically significant.

383

bioRxiv preprint doi: https://doi.org/10.1101/2021.08.04.455154; this version posted August 4, 2021. The copyright holder for this preprint (which was not certified by peer review) is the author/funder. All rights reserved. No reuse allowed without permission.

384 **Results**

385 **Inhibition of p38α reduces TDP-43 aggregation, phosphorylation, and toxicity**

386 Several lines of evidence point to a role for p38 MAPK in the development and progression of ALS
387 (Bendotti et al., 2004; Corrêa and Eales, 2012; Gibbs et al., 2018; Tortarolo et al., 2003; Zhan et al.,
388 2015). Thus, we first asked whether p38α modulates the formation of insoluble TDP-43 aggregates
389 in human neuronal SH-SY5Y cells. Increased expression of wild-type or ALS-linked TDP-43 variants
390 elicits ALS-like phenotypes in various *in vitro* and *in vivo* models (Arnold et al., 2013; Johnson et
391 al., 2009; Watkins et al., 2020; Wobst et al., 2017; Xu et al., 2011). Indeed, elevated expression of
392 wild-type TDP-43 is connected with FTD (Gitcho et al., 2009) and disease-linked TDP-43
393 aggregation is proposed to increase TDP-43 expression due to loss of TDP-43 autoregulation (Gasset-
394 Rosa et al., 2019; Polymenidou et al., 2011). TDP-43^{M337V}, a pathological mutant form of TDP-43
395 associated with fALS, has been shown to be especially aggregation-prone and highly phosphorylated
396 (Johnson et al., 2009; Sreedharan et al., 2008; Wobst et al., 2017). We therefore used the TDP-43^{M337V}
397 variant in our experiments to detect more prominent changes in TDP-43 solubility and
398 phosphorylation, and to maximize our experimental signal window. Using siRNA-mediated
399 knockdown of p38α and TDP-43^{M337V} expression, we monitored the accumulation of total and
400 phosphorylated TDP-43 (pTDP-43) in RIPA- or urea-soluble fractions over time. We found that the
401 depletion of p38α significantly reduced the accumulation of insoluble TDP-43^{M337V} in the urea
402 fraction at all time points (Figure 1B-1C). Thus, reduction of p38α reduces TDP-43 aggregation in
403 human neuronal cells.

404

405 Phosphorylation of S409 and S410 of TDP-43 is a consistent feature in all sporadic and familial forms
406 of TDP-43 proteinopathies (Neumann et al., 2009). TDP-43 is phosphorylated at S409/S410 in
407 pathological inclusions, but S409/S410 phosphorylation is not observed under physiological
408 conditions in the nucleus (Neumann et al., 2009). Interestingly, we observed a marked decrease in

bioRxiv preprint doi: https://doi.org/10.1101/2021.08.04.455154; this version posted August 4, 2021. The copyright holder for this preprint (which was not certified by peer review) is the author/funder. All rights reserved. No reuse allowed without permission.

409 pTDP-43 (i.e. TDP-43 phosphorylated at S409/S410) in the urea fraction when p38α is knocked down
410 (Figure 1B and 1D). Similarly, increased expression of TDP-43^{WT}, in place of TDP-43^{M337V}, or using
411 a different siRNA to knockdown p38α also decreased pTDP-43 in the urea fraction (Figure S1). Thus,
412 reduction of p38α reduces TDP-43 aggregation and pathological phosphorylation of S409/S410 in
413 human neuronal cells.
414
415 Next, we assessed whether pharmacological inhibition of p38α activity affects the solubility and the
416 phosphorylation status of TDP-43 in a similar manner to genetic ablation. Indeed, treatment of SH-
417 SY5Y cells with the p38α inhibitor, compound 1 (see Materials and Methods), significantly reduced
418 TDP-43^{M337V} phosphorylation and aggregation, in a concentration- and time-dependent manner
419 (Figure 1E-1H). Note that we only observe TDP-43 phosphorylation at S409/S410 in the insoluble
420 urea fraction and not in the soluble RIPA fraction (Figure 1E), indicating the pathological nature of
421 S409/S410 phosphorylation. Our findings suggest that p38α inhibition is an effective strategy to
422 reduce pathological TDP-43 aggregation and phosphorylation.
423
424 To test whether p38α pharmacological inhibition affects toxicity induced by increased TDP-43
425 expression, we performed an LDH cytotoxicity assay in mouse motor-neuron-like NSC-34 cells.
426 Expression of TDP-43^{WT} (Figure 1I) or TDP-43^{M337V} in NSC-34 cells induces cytotoxicity.
427 Importantly, inhibition of p38α by compound 1 significantly rescued TDP-43^{WT}-induced cytotoxicity
428 (Figure 1I). Thus, pharmacological inhibition of p38α mitigates TDP-43 toxicity in motor-neuron-
429 like NSC-34 cells.
430
431 To determine whether p38α pharmacological inhibition rescues TDP-43-induced neurodegeneration,
432 we employed a longitudinal imaging system to monitor neuronal survival (Barmada et al., 2010). We
433 cultured primary mouse cortical neurons, uniformly labeled them with a fluorescent protein

bioRxiv preprint doi: https://doi.org/10.1101/2021.08.04.455154; this version posted August 4, 2021. The copyright holder for this preprint (which was not certified by peer review) is the author/funder. All rights reserved. No reuse allowed without permission.

434 (mApple), and expressed TDP43^{M337V}. We imaged and tracked the neurons daily for 7 days and used
435 Cox proportional hazard analysis to measure the cumulative risk of death and hazard ratios. We have
436 previously shown that this assay is very sensitive to detecting TDP-43-induced neurodegeneration
437 (Barmada et al., 2010). We found that treatment of neurons with a brain-penetrant p38α
438 pharmacological inhibitor, VX-745 (also known as Neflamapimod) (Duffy et al., 2011), which is in
439 phase 2 clinical trials for Alzheimer's disease, Huntington's disease, and dementia with Lewy bodies
440 (Germann and Alam, 2020; Prins et al., 2021), significantly reduced the hazard ratio of TDP-43^{M337V}-
441 expressing neurons (Figure 1J). Thus, clinical stage, brain-penetrant p38α inhibitors can also mitigate
442 TDP-43 neurotoxicity. Taken together, our results demonstrate that p38α inhibition reduces the
443 pathological aggregation and phosphorylation of TDP-43, and mitigates TDP-43 toxicity in multiple
444 settings.

445

446 **Constitutively active p38α promotes TDP-43 aggregation, S409/S410 phosphorylation, and**
447 **cytoplasmic accumulation**

448 The siRNA knockdown experiments demonstrated that p38α depletion reduces TDP-43 aggregation
449 and phosphorylation at S409/S410. Therefore, we hypothesized that p38α overexpression would
450 increase TDP-43 aggregation and phosphorylation. To test our hypothesis, we co-expressed TDP-
451 43^{M337V} with wild-type, constitutively active (CA), or dominant negative (DN) forms of p38α in SH-
452 SY5Y cells. Expression of WT or DN-p38α did not have any significant effect on S409/S410
453 phosphorylation or accumulation of TDP-43 in the urea fraction (Figure 2A-2D). By contrast, CA-
454 p38α promoted TDP-43^{M337V} aggregation, as evidenced by the accumulation of TDP-43 in the urea
455 fraction (Figure 2A-2D). CA-p38α also significantly increased TDP-43 phosphorylation at
456 S409/S410 (Figure 2A-2D). Thus, p38α activation promotes pathological TDP-43 phosphorylation
457 and aggregation.

458

bioRxiv preprint doi: https://doi.org/10.1101/2021.08.04.455154; this version posted August 4, 2021. The copyright holder for this preprint (which was not certified by peer review) is the author/funder. All rights reserved. No reuse allowed without permission.

459 Next, we assessed whether TDP-43^{M337V} co-localizes with p38α in cells. Previously, TDP-43^{M337V}
460 and p38α have been detected in ubiquitinated inclusions (Bendotti et al., 2004; Wobst et al., 2017).
461 Interestingly, we found a significant increase in the number of cells displaying intranuclear TDP-
462 43^{M337V} inclusions specifically when CA-p38α was co-expressed (Figure 2E-2F). Furthermore, these
463 intranuclear TDP-43 inclusions stained positive for p38α (Figure 2E). We also found that expression
464 of CA-p38α promoted the cytoplasmic accumulation of TDP-43, as shown by an increase of TDP-43
465 in the cytoplasmic fraction (Figure 2G-2H). Together, our data demonstrate that aberrant activation
466 of p38α promotes several hallmarks of ALS pathology, including TDP-43 aggregation,
467 phosphorylation at S409/S410, and cytoplasmic accumulation.
468

469 **TDP-43 is directly phosphorylated by p38α at residues S292, S409, and S410**

470 Co-localization of TDP-43 and CA-p38α in intranuclear aggregates might indicate a physical
471 interaction between TDP-43 and p38α (Figure 2E). To explore this possibility, we transfected SH-
472 SY5Y with TDP-43^{WT} and p38α, and then immunoprecipitated p38α or TDP-43 (Figure 3A). TDP-
473 43^{WT} and p38α co-immunoprecipitated in both reciprocal immunoprecipitation experiments,
474 suggesting a robust interaction between TDP-43 and p38α (Figure 3A). Consistently, siRNA-
475 mediated knockdown of p38α reduced the amount of pulled down pTDP-43, and also diminished the
476 amount of endogenous p38α that co-immunoprecipitated with TDP-43^{M337V} (Figure S2), further
477 validating an interaction between p38α and TDP-43.
478

479 Next, we asked whether TDP-43 is directly phosphorylated by p38α. Thus, we performed *in vitro*
480 kinase assays. Samples containing recombinant wild-type TDP-43 with or without active p38α were
481 analyzed by western blot analysis after a 30-minute incubation period. In the absence of p38α, no
482 phosphorylation was detected at the S409/S410 site (Figure 3B). However, in the presence of active
483 kinase, a robust band of phosphorylated TDP-43 was observed, indicating that TDP-43 is directly

bioRxiv preprint doi: https://doi.org/10.1101/2021.08.04.455154; this version posted August 4, 2021. The copyright holder for this preprint (which was not certified by peer review) is the author/funder. All rights reserved. No reuse allowed without permission.

484 phosphorylated by p38α at S409/S410 (Figure 3B). As expected, the phosphorylation of TDP-43 was
485 prevented by pharmacological inhibition of p38α with compound 1 (Figure 3B).
486
487 While S409/S410 residues are thought to be the major pathological phosphorylation sites in TDP-43
488 (Neumann et al., 2009), we sought to investigate whether p38α phosphorylates TDP-43 at additional
489 serine or threonine residues. Therefore, we performed LC-MS/MS analysis of trypsin-digested TDP-
490 43 after incubation with p38α, which revealed that p38α also phosphorylates TDP-43 at serine residue
491 292 (S292) (Figure 1A). In fact, TDP-43 is phosphorylated at S292 in the brains of ALS patients
492 (Kametani et al., 2016). Furthermore, a serine-to-asparagine mutation at this site (S292N) is
493 genetically linked to sALS and fALS (Harrison and Shorter, 2017; Xiong et al., 2010; Zou et al.,
494 2012). To investigate the potential effects of phosphorylation at S292 on the aggregation propensity
495 of TDP-43, we took a site-directed mutagenesis approach to generate phospho-mimetic (S292E; TDP-
496 43^{S292E}), phospho-dead (S292A; TDP-43^{S292A}), and ALS-linked (S292N; TDP-43^{S292N}) TDP-43
497 mutants, which were transfected into SH-SY5Y cells. We compared the aggregation propensity of
498 these S292 mutants to that of TDP-43^{WT} and TDP-43 variants harboring S409:S410A (TDP-
499 $43^{S409:S410A}$), S409:S410E (TDP-$43^{S409:S410E}$) and S292:S409:S410A (TDP-$43^{S292:S409:S410A}$)
500 mutations. Interestingly, overexpressing the phospho-mimetic mutant TDP-43^{S292E} increased the
501 aggregation propensity of TDP-43, as evidenced by the accumulation of TDP-43 in the urea fraction,
502 and also enhanced its phosphorylation at serine residues 409/410 (Figure 3C and 3D). Moreover,
503 TDP-43^{S292E} enhanced the formation of 35 kDa C-terminal fragments of TDP-43 (CTF), which are
504 associated with TDP-43 proteinopathy (Buratti, 2018) (Figure 3C and 3E). Neither TDP-43^{S292A},
505 TDP-43^{S292N}, TDP-$43^{S409:S410A}$, TDP-$43^{S409:S410E}$ nor TDP-$43^{S292:S409:S410A}$ had any significant effect
506 on TDP-43 aggregation propensity compared to TDP-43^{WT} (Figure 3C-3D). These results suggest
507 that aggregation of TDP-43 may be enhanced by S292 phosphorylation in neuronal cells. Moreover,
508 S292 phosphorylation also likely stimulates phosphorylation at S409/410.

bioRxiv preprint doi: https://doi.org/10.1101/2021.08.04.455154; this version posted August 4, 2021. The copyright holder for this preprint (which was not certified by peer review) is the author/funder. All rights reserved. No reuse allowed without permission.

509 **TDP-43 undergoes arginine methylation catalyzed by PRMT1**

510 Our data suggest a role for S292 in regulating TDP-43 aggregation via p38α-mediated
511 phosphorylation. An alignment of TDP-43 amino acid sequences revealed that S292 is highly
512 conserved across the phylogenic spectrum from *Homo sapiens* to *Gallus gallus* (Figure 4A).
513 Intriguingly, an arginine-glycine-glycine (RGG) motif directly follows the S292 residue and is also
514 highly conserved (Figure 4A). RGG/RG motifs are preferred substrates for methylation by members
515 of the PRMT family (Thandapani et al., 2013). Given that several studies have shown that arginine
516 methylation can attenuate phosphorylation at nearby residues on the same protein (Guo et al., 2010;
517 Hsu et al., 2011; Lu et al., 2017; Yamagata et al., 2008), we hypothesized that arginine methylation
518 at R293 could potentially interfere with p38α-mediated phosphorylation at the adjacent residue S292.
519 Recent proteomic studies have found that TDP-43 is methylated in HCT116 and HEK293 cells as
520 well as in mouse embryos and human brain tissue (Guo et al., 2014; Larsen et al., 2016). To assess
521 TDP-43 arginine methylation in SH-SY5Y cells, we immunoprecipitated endogenous TDP-43 and
522 probed using antibodies against monomethyl-arginine (MMA), asymmetric dimethyl-arginine
523 (ADMA) or symmetric dimethyl-arginine (SDMA). Western blot analysis showed that
524 immunoprecipitated TDP-43 was indeed mono- and asymmetrically dimethylated and was efficiently
525 recognized by the MMA and ADMA antibodies, but not a SDMA antibody (Figure 4B). Critically,
526 when we depleted PRMT1, the most abundant PRMT in mammalian cells (Tang et al., 2000), using
527 siRNA-mediated knockdown in SH-SY5Y cells, followed by TDP-43 immunoprecipitation and
528 western blot analysis, we found a significant decrease in methylation of endogenous TDP-43 (Figure
529 4C). Additionally, treating cells with AdOx, a global methyltransferase inhibitor, for 24 hours
530 significantly decreased the methylation of overexpressed TDP-43^{WT}, evident by a decrease in
531 immunoprecipitated TDP-43 detected by anti-MMA and anti-ADMA (Figure 4D). Collectively, these
532 data suggest that PRMT1 methylates TDP-43.

533

bioRxiv preprint doi: https://doi.org/10.1101/2021.08.04.455154; this version posted August 4, 2021. The copyright holder for this preprint (which was not certified by peer review) is the author/funder. All rights reserved. No reuse allowed without permission.

534 Next, we wanted to verify whether R293 is the targeted residue for arginine methylation. Using site-
535 directed mutagenesis, we generated a methylation-dead mutant of TDP-43 by substituting the arginine
536 residue at 293 to a lysine (TDP-43^{R293K}). Unlike for TDP-43^{WT}, immunoprecipitating TDP-43^{R293K}
537 and probing for monomethylated TDP-43 using anti-MMA antibody revealed an absence of
538 monomethylated TDP-43 (Figure 4E). Overall, our results provide evidence that PRMT1 methylates
539 TDP-43 at R293 in human neuronal cells.

540

541 **TDP-43 arginine methylation favors normal LLPS over aberrant aggregation**

542 Arginine methylation of TDP-43 has been largely unexplored. Thus, little is known about R293
543 methylation and whether it affects TDP-43 LLPS or aggregation propensity at the pure protein level.
544 Likewise, we have limited understanding of how specific phosphorylation events might affect TDP-
545 43 LLPS and aggregation at the pure protein level. To address how phosphorylation and methylation
546 can alter TDP-43 LLPS behavior, we first performed *in vitro* droplet formation assays. Purified
547 recombinant maltose-binding protein (MBP)-tagged TDP-43^{WT}, the phospho-mimicking mutants
548 TDP-43^{S292E}, TDP-43$^{S409:S410E}$, TDP-43$^{S292:S409:S410E}$, and the arginine methylation-mimic TDP-
549 43^{R293F} (Campbell et al., 2012; Huq et al., 2006; Liu et al., 2019), were separately incubated at
550 physiological concentration (10μM) (Ling et al., 2010) in phase separation buffer containing
551 physiological salt concentration and 10% (w/v) dextran to mimic the crowded cellular environment
552 (Mann et al., 2019; McGurk et al., 2018). Formation of TDP-43 droplets was then visualized using
553 DIC microscopy. TDP-43^{WT} formed spherical droplets that were relatively large in size (average area
554 of ~12.6μm^2 ± 1.3), and capable of fusion events indicating liquid-like properties (Figure 5A-C). In
555 contrast, all three phosphomimetic TDP-43 mutants partitioned into droplets that were smaller in size
556 (TDP-43^{S292E}, ~5.8μm^2 ± 0.6; TDP-43$^{S409:S410E}$, ~3.9μm^2 ± 0.3; and TDP-43$^{S292:S409:S410E}$, ~3.2 μm^2 ±
557 0.2) compared to those of TDP-43^{WT} (Figure 5A-C). There was no change in the number of droplets
558 between mutants and TDP-43^{WT}. Thus, these reductions in droplet sizes suggest that phosphorylation

bioRxiv preprint doi: https://doi.org/10.1101/2021.08.04.455154; this version posted August 4, 2021. The copyright holder for this preprint (which was not certified by peer review) is the author/funder. All rights reserved. No reuse allowed without permission.

559 of S292, S409, and S410 may limit the LLPS propensity of TDP-43. Interestingly, the arginine-
560 methylation mimic, TDP-43^{R293F}, formed large droplets that were comparable to TDP-43^{WT}
561 (~12.6µm^2 ± 1.9) (Figure 5A-C). These results indicated that phosphorylation and methylation likely
562 have contrasting effects on LLPS of TDP-43. Thus, R293 methylation likely permits wild-type levels
563 of TDP-43 LLPS, whereas S292, S409, and S410 phosphorylation likely reduce TDP-43 LLPS.
564
565 Given these outcomes, we next compared the effects of phosphorylation and methylation mimics on
566 TDP-43 aggregation propensity using an *in vitro* aggregation assay. Recombinant TDP-43-MBP
567 protein constructs were incubated with TEV protease and their aggregation was monitored over time.
568 Under these conditions, selective cleavage of the MBP tag by TEV protease results in the formation
569 of solid-phase TDP-43 aggregates and fibrils (Cook et al., 2020), indicated by an increase in turbidity.
570 Here, we found that there were only minor differences in aggregation between TDP-43^{WT} and the
571 phosphomimics TDP-43^{S292E} and TDP-43$^{S409E:S410E}$ (Figure 5D). By contrast, the phosphomimic
572 TDP-43$^{S292E:S409E:S410E}$ and the arginine methylation mimic, TDP-43^{R293F}, exhibited modestly reduced
573 aggregation (Figure 5D). However, compared to TDP-43^{WT} this reduced aggregation was only
574 significant for TDP-43^{R293F} (Figure 5E). Strikingly, plotting the normalized aggregation against the
575 LLPS propensities of TDP-43^{WT} and its mutant forms, we found that the phosphomimetic mutants
576 have a relatively higher tendency for aggregation over LLPS (Figure 5F). By contrast, TDP-43^{R293F}
577 has a relatively higher tendency to undergo LLPS over aggregation (Figure 5F). Taken together, our
578 results imply that TDP-43 phosphorylation and methylation may have opposing effects on TDP-43
579 (Figure 5F). Phosphorylation at S292, S409, and S410 reduces the propensity for TDP-43 to undergo
580 LLPS, but has limited effects on TDP-43 aggregation (Figure 5G). Thus, S292, S409, and S410
581 phosphorylation may divert TDP-43 toward aggregation and away from LLPS (Figure 5G). This
582 finding could explain why phosphorylated TDP-43 accumulates as aggregates in the urea fraction in
583 cells. In contrast, R293 methylation allows TDP-43 to undergo normal LLPS, but reduces TDP-43

bioRxiv preprint doi: https://doi.org/10.1101/2021.08.04.455154; this version posted August 4, 2021. The copyright holder for this preprint (which was not certified by peer review) is the author/funder. All rights reserved. No reuse allowed without permission.

584 aggregation (Figure 5G). Thus, R293 methylation may reduce the propensity of TDP-43 to aggregate
585 and enter the urea fraction in cells.
586

587 **Arginine methylation regulates TDP-43 aggregation in human neuronal cells**

588 We next investigated the impact of arginine methylation on TDP-43 in a cellular context. SH-SY5Y
589 cells were treated with AdOx, an arginine methyltransferase inhibitor, followed by fractionation and
590 western blot analysis. We found that global methyltransferase inhibition promoted the accumulation
591 of TDP-43 in the urea fraction (Figure 6A and B). Conversely, the overexpression of PRMT1 led to
592 a decrease in TDP-43 aggregation, evident by a decrease of total and phosphorylated TDP-43 in the
593 urea fraction (Figure 6C and D). To further investigate the effect of hypomethylation on TDP-43
594 aggregation, we next mutated TDP-43 to have an additional RGG motif (TDP-43^{G308R}) (Figure 4A).
595 Based on previous studies, the introduction of an additional RGG motif has led to the
596 hypomethylation and subsequent aggregation of another ALS-linked RBP, FUS (Qamar et al., 2018).
597 Accordingly, we found that TDP-43^{G308R} significantly accumulated in the urea fraction and was more
598 highly phosphorylated at S409/S410, compared to TDP-43^{WT} (Figure 6E and F). Together, these
599 findings suggest that arginine methylation exerts a protective role on TDP-43, perhaps by decreasing
600 its aggregation propensity via regulation of phosphorylation.
601

602 **Crosstalk between TDP-43 arginine methylation and p38α-mediated phosphorylation**

603 The observation that TDP-43 undergoes PRMT1-mediated arginine methylation at the R293 site,
604 coupled with our purified protein data suggesting contrasting outcomes between TDP-43
605 phosphorylation and methylation, led us to ask whether phosphorylation at S292 interferes with
606 arginine methylation at the adjacent residue, R293, or vice versa (Figure 4A). To answer this question,
607 we expressed flag-tagged TDP-43^{WT} as well as TDP-43^{S292E}, TDP-43^{S292N}, and TDP-43^{S292A} mutants
608 in SH-SY5Y cells and analyzed their methylation status. Immunoprecipitation followed by

bioRxiv preprint doi: https://doi.org/10.1101/2021.08.04.455154; this version posted August 4, 2021. The copyright holder for this preprint (which was not certified by peer review) is the author/funder. All rights reserved. No reuse allowed without permission.

609 immunoblotting revealed a striking reduction in the MMA-signal in the phospho-mimicking TDP-
610 43^{S292E} mutant (Figure 7A). Interestingly, when compared to $TDP\text{-}43^{WT}$, the ALS-linked $TDP\text{-}43^{S292N}$
611 mutant showed a modest decrease in MMA-levels, whereas the $TDP\text{-}43^{S292A}$ mutant did not show
612 any difference (Figure 7A). As shown previously (Figure 3C), the $TDP\text{-}43^{S292E}$ mutant also promoted
613 phosphorylation of TDP-43 at S409/S410, further underlining the anti-correlative relationship
614 between TDP-43 arginine methylation and S409/S410 phosphorylation (Figure 7A). These
615 observations suggest that phosphorylation at S292, possibly combined with increased
616 phosphorylation at S409/S410, could interfere with TDP-43 methylation. However, these findings do
617 not rule out that a reduction in TDP-43 methylation could be due to steric hindrance caused by the
618 glutamic acid residue at position 292.
619
620 To further define the relationship between these two PTMs, we studied the methylation status of TDP-
621 43 after genetic depletion of p38α. As shown previously (Figure 1B), we found that p38α
622 downregulation reduced the phosphorylation of $TDP\text{-}43^{WT}$ at S409/S410 (Figure 7B). Interestingly,
623 western blot analysis also revealed that p38α depletion significantly decreased the formation of the
624 ~35 kDa TDP-43-CTF (Figure 7B and C), and resulted in elevated levels of mono-methylated TDP-
625 43-CTF (Figure 7B and D). These observations suggest that there is an interplay between arginine
626 methylation and p38α-mediated phosphorylation, and that reduced p38α activity could increase TDP-
627 43 arginine methylation. Indeed, we found that overexpression of PRMT1 led to a strong increase in
628 mono-methylated TDP-43-CTF and a striking reduction in TDP-43 phosphorylation at S409/S410
629 (Figure 7E), further corroborating the hypothesis that there is crosstalk between TDP-43 arginine
630 methylation and phosphorylation at disease-relevant residues.
631
632

bioRxiv preprint doi: https://doi.org/10.1101/2021.08.04.455154; this version posted August 4, 2021. The copyright holder for this preprint (which was not certified by peer review) is the author/funder. All rights reserved. No reuse allowed without permission.

633 **Discussion**

634 Since the discovery that ~97% of ALS cases and ~50% of FTD cases present with TDP-43
635 proteinopathy (Arai et al., 2006; Harrison and Shorter, 2017; Neumann et al., 2006), TDP-43 has
636 been subject to much investigation. However, the mechanisms leading to an accumulation of
637 insoluble TDP-43 aggregates are not yet fully understood. Aberrant TDP-43 phosphorylation is one
638 of the major distinguishing pathological features of TDP-43 inclusions in human brains (Hasegawa
639 et al., 2008; Neumann et al., 2009). Although the consequences of these phosphorylation events have
640 not been unequivocally established, aberrant phosphorylation of TDP-43 is associated with
641 cytoplasmic mislocalization, decreased solubility, aberrant cleavage and cytotoxicity (Barmada et al.,
642 2010; Brady et al., 2011; Kim et al., 2015; Liachko et al., 2010; Nonaka et al., 2009; Zhang et al.,
643 2010). To date, casein kinases CK1 and CK2, CDC7 and TTBK1/2 have been shown to phosphorylate
644 TDP-43 *in vitro* and *in vivo,* and promote its pathological aggregation and neurotoxicity (Carlomagno
645 et al., 2014; Choksi et al., 2014; Goh et al., 2018; Kametani et al., 2009; Liachko et al., 2013, 2014;
646 Liu et al., 2015; Meyerowitz et al., 2011; Nonaka et al., 2016; Sreedharan et al., 2015; Taylor et al.,
647 2018). However, some studies have found that hyperphosphorylation of the TDP-43 PrLD can reduce
648 TDP-43 LLPS and aggregation (Li et al., 2011; Silva et al., 2021), indicating a complex interplay
649 between combinatorial TDP-43 PTMs and pathology. Importantly, increased activation of the MAP
650 kinase p38 has been detected in human post-mortem ALS tissue, which is further substantiated by the
651 findings that persistent activation of the p38 signaling pathways induce neurodegeneration (Bendotti
652 et al., 2004; Dewil et al., 2007; Tortarolo et al., 2003). However, until now, the effect of p38α on
653 TDP-43 specifically has not been explored.

654

655 In this study, we elucidated the impact of p38α on TDP-43 proteinopathy. Using neuronal cells, we
656 first showed that genetic depletion and pharmacological inhibition of p38α suppressed TDP-43
657 phosphorylation, aggregation, and toxicity. We further established that TDP-43 is a substrate of p38α-

bioRxiv preprint doi: https://doi.org/10.1101/2021.08.04.455154; this version posted August 4, 2021. The copyright holder for this preprint (which was not certified by peer review) is the author/funder. All rights reserved. No reuse allowed without permission.

658 mediated phosphorylation. Using *in vitro* biochemical assays followed by LC-MS/MS we established
659 that TDP-43 is directly phosphorylated by p38α at residues S292, and S409/S410. Intriguingly,
660 mutations at S292 have been linked to pathogenicity in both sporadic and familial ALS. However, no
661 biochemical mechanistic data have been reported on the effect of this mutation (Xiong et al., 2010;
662 Zou et al., 2012). Here, we demonstrated that the phospho-mimetic mutant TDP-43^{S292E} significantly
663 promoted phosphorylation of TDP-43 at S409/S410 and enhanced the accumulation of insoluble
664 TDP-43 aggregates. These findings identified S292 as a major site for TDP-43 phospho-regulation.
665 Interestingly, we found that S292, and the RGG-motif immediately following this residue are highly
666 conserved across the phylogenic spectrum. The RGG-motif presents a major site for methylation by
667 members of the PRMT family (Chang et al., 2011; Huang et al., 2018; Thandapani et al., 2013; Wall
668 and Lewis, 2017), and we show here that R293 is a major site for methylation by PRMT1 in human
669 neuronal cells. This result supports earlier proteomic studies of mouse embryonic and brain tissue
670 indicating that TDP-43 can be methylated at R293 (Guo et al., 2014; Larsen et al., 2016). Furthermore,
671 recent evidence also corroborates the possible role of arginine methylation in neurodegeneration.
672 Specifically, PRMT1 was identified as a significant modulator of toxicity in C9-ALS (Ortega et al.,
673 2020).
674
675 There is increasing evidence suggesting that phosphorylation and arginine methylation co-exist on
676 the same protein, and that these PTMs can have opposing or potentiating effects on protein function
677 (Basso and Pennuto, 2015; Lu et al., 2017). For example, the functions of p16 protein are regulated
678 by the antagonistic crosstalk between arginine methylation at residue R138 and phosphorylation at
679 residue S140 (Lu et al., 2017). Here, we provide similar evidence for the crosstalk between PRMT1-
680 catalyzed arginine methylation at R293 and p38α-mediated phosphorylation at the adjacent residue
681 S292 in the regulation of TDP-43 LLPS and aggregation. Our *in vitro* and *in vivo* data elucidate a
682 dichotomous relationship between methylation and phosphorylation of TDP-43. Perhaps as a

bioRxiv preprint doi: https://doi.org/10.1101/2021.08.04.455154; this version posted August 4, 2021. The copyright holder for this preprint (which was not certified by peer review) is the author/funder. All rights reserved. No reuse allowed without permission.

683 protective mechanism, TDP-43 methylation at R293 reduces phosphorylation at S292 and
684 S409/S410, which in turn reduces TDP-43 aggregation. Conversely, the phosphomimetic S292E
685 reduces the levels of TDP-43 methylation. Our biochemical studies suggest that S292 and S409/S410
686 phosphorylation render TDP-43 less prone to undergo LLPS, which may divert TDP-43 along
687 pathological aggregation trajectories (Conicella et al., 2016). Whether TDP-43 methylation at R293
688 inhibits phosphorylation at S292, or vice versa, due to steric hindrance have yet to be further
689 investigated. Nevertheless, our study suggests for the first time an intricate interplay between protein
690 phosphorylation and arginine methylation in the regulation of TDP-43. While additional studies will
691 be necessary to further clarify the dynamics of these regulatory processes, especially in the context
692 of more complex, clinically-relevant models, our study provides a platform for developing novel
693 therapeutic strategies to inhibit p38α or promote PRMT1 activity to rescue TDP-43 pathologies
694 associated with ALS/FTD. Indeed, it is interesting to note that the brain-penetrant p38α inhibitor,
695 VX-745, which mitigates TDP-43 toxicity in primary neurons (Figure 1J), has reached phase 2
696 clinical trials for Alzheimer's disease, Huntington's disease, and dementia with Lewy bodies
697 (Germann and Alam, 2020; Prins et al., 2021). Our data indicate that VX-745 might also be
698 considered as a clinical candidate for ALS/FTD that presents with TDP-43 proteinopathy. Indeed, we
699 suggest that strategies to reduce p38α-mediated TDP-43 phosphorylation and promote R293
700 methylation could have therapeutic utility for ALS/FTD and other TDP-43 proteinopathies.
701

702 **Acknowledgements**

703 We thank Charlotte Fare and Katie Copley for feedback on the manuscript, and Rebecca Jarvis for
704 small-molecule curation. MA and HMO were supported by the AstraZeneca postdoctoral fellowships.
705 BC was a member of the AstraZeneca graduate program. KLM was supported by supported by a NSF
706 graduate research fellowship (DGE-1321851). AFF was supported by NIH grants T32AG00255 and
707 F31NS087676. EMB was supported by a Milton Safenowitz Post-Doctoral Fellowship from the ALS

bioRxiv preprint doi: https://doi.org/10.1101/2021.08.04.455154; this version posted August 4, 2021. The copyright holder for this preprint (which was not certified by peer review) is the author/funder. All rights reserved. No reuse allowed without permission.

708 Association and NIH grant F32NS108598. RRC was supported by NIH grants T32GM008275,
709 F31AG060672, and a Blavatnik Family Fellowship in Biomedical Research. JS was supported by
710 Target ALS, The Association for Frontotemporal Degeneration, The Packard Foundation for ALS
711 research, The ALS Association, The G. Harold and Leila Y. Mathers Charitable Foundation, the
712 Office of the Assistant Secretary of Defense for Health Affairs (USA), through the Amyotrophic
713 Lateral Sclerosis Research Program (W81XWH-20-1-0242), and NIH grants R01GM099836 and
714 R21AG065854. This work was supported by a grant to NJB, DGB, JS, ADG, SF from the Target
715 ALS Foundation and ALS Finding a Cure.

716

717 **Conflict of interest**

718 HJW, DGB, and NJB were all full-time employees and shareholders of AstraZeneca at the time these
719 studies were conducted. SJM serves as a consultant for SAGE Therapeutics and AstraZeneca,
720 relationships that are regulated by Tufts University. JS is a consultant for Dewpoint Therapeutics,
721 Maze Therapeutics, Vivid Sciences, Korro Bio, and ADRx.

722

bioRxiv preprint doi: https://doi.org/10.1101/2021.08.04.455154; this version posted August 4, 2021. The copyright holder for this preprint (which was not certified by peer review) is the author/funder. All rights reserved. No reuse allowed without permission.

723 **References**

724 Alami, N.H., Smith, R.B., Carrasco, M.A., Williams, L.A., Winborn, C.S., Han, S.S.W., Kiskinis,
725 E., Winborn, B., Freibaum, B.D., Kanagaraj, A., et al. (2014). Axonal Transport of TDP-43 mRNA
726 Granules Is Impaired by ALS-Causing Mutations. Neuron *81*, 536–543.

727 Arai, T., Hasegawa, M., Akiyama, H., Ikeda, K., Nonaka, T., Mori, H., Mann, D., Tsuchiya, K.,
728 Yoshida, M., Hashizume, Y., et al. (2006). TDP-43 is a component of ubiquitin-positive tau-
729 negative inclusions in frontotemporal lobar degeneration and amyotrophic lateral sclerosis.
730 Biochem Bioph Res Co *351*, 602–611.

731 Arnold, E.S., Ling, S.-C., Huelga, S.C., Lagier-Tourenne, C., Polymenidou, M., Ditsworth, D.,
732 Kordasiewicz, H.B., McAlonis-Downes, M., Platoshyn, O., Parone, P.A., et al. (2013). ALS-linked
733 TDP-43 mutations produce aberrant RNA splicing and adult-onset motor neuron disease without
734 aggregation or loss of nuclear TDP-43. Proc National Acad Sci *110*, E736–E745.

735 Arrasate, M., and Finkbeiner, S. (2005). Automated microscope system for determining factors that
736 predict neuronal fate. P Natl Acad Sci Usa *102*, 3840–3845.

737 Aulas, A., Stabile, S., and Velde, C.V. (2012). Endogenous TDP-43, but not FUS, contributes to
738 stress granule assembly via G3BP. Mol Neurodegener *7*, 1.

739 Ayala, Y.M., Zago, P., D'Ambrogio, A., Xu, Y.-F., Petrucelli, L., Buratti, E., and Baralle, F.E.
740 (2008). Structural determinants of the cellular localization and shuttling of TDP-43. J Cell Sci *121*,
741 3778–3785.

742 Barmada, S.J., Skibinski, G., Korb, E., Rao, E.J., Wu, J.Y., and Finkbeiner, S. (2010). Cytoplasmic
743 Mislocalization of TDP-43 Is Toxic to Neurons and Enhanced by a Mutation Associated with
744 Familial Amyotrophic Lateral Sclerosis. J Neurosci *30*, 639–649.

745 Basso, M., and Pennuto, M. (2015). Serine phosphorylation and arginine methylation at the
746 crossroads to neurodegeneration. Exp Neurol *271*, 77–83.

747 Beausoleil, S.A., Villén, J., Gerber, S.A., Rush, J., and Gygi, S.P. (2006). A probability-based
748 approach for high-throughput protein phosphorylation analysis and site localization. Nat Biotechnol
749 *24*, 1285–1292.

750 Bendotti, C., Atzori, C., Piva, R., Tortarolo, M., Strong, M.J., Debiasi, S., and Migheli, A. (2004).
751 Activated p38MAPK Is a Novel Component of the Intracellular Inclusions Found in Human
752 Amyotrophic Lateral Sclerosis and Mutant SOD1 Transgenic Mice. J Neuropathology Exp
753 Neurology *63*, 113–119.

754 Brady, O.A., Meng, P., Zheng, Y., Mao, Y., and Hu, F. (2011). Regulation of TDP-43 aggregation
755 by phosphorylation andp62/SQSTM1. J Neurochem *116*, 248–259.

756 Brennan, C.M., Emerson, C.P., Owens, J., and Christoforou, N. (2021). p38 MAPKs — roles in
757 skeletal muscle physiology, disease mechanisms, and as potential therapeutic targets. Jci Insight *6*,
758 e149915.

bioRxiv preprint doi: https://doi.org/10.1101/2021.08.04.455154; this version posted August 4, 2021. The copyright holder for this preprint (which was not certified by peer review) is the author/funder. All rights reserved. No reuse allowed without permission.

759 Buratti, E. (2018). TDP-43 post-translational modifications in health and disease. Expert Opin Ther
760 Tar *22*, 279–293.

761 Buratti, E., and Baralle, F.E. (2008). Multiple roles of TDP-43 in gene expression, splicing
762 regulation, and human disease. Front Biosci *13*, 867.

763 Buratti, E., Brindisi, A., Giombi, M., Tisminetzky, S., Ayala, Y.M., and Baralle, F.E. (2005). TDP-
764 43 Binds Heterogeneous Nuclear Ribonucleoprotein A/B through Its C-terminal Tail AN
765 IMPORTANT REGION FOR THE INHIBITION OF CYSTIC FIBROSIS TRANSMEMBRANE
766 CONDUCTANCE REGULATOR EXON 9 SPLICING*. J Biol Chem *280*, 37572–37584.

767 Burton, J.C., Antoniades, W., Okalova, J., Roos, M.M., and Grimsey, N.J. (2021). Atypical p38
768 Signaling, Activation, and Implications for Disease. Int J Mol Sci *22*, 4183.

769 Campbell, M., Chang, P.-C., Huerta, S., Izumiya, C., Davis, R., Tepper, C.G., Kim, K.Y.,
770 Shevchenko, B., Wang, D.-H., Jung, J.U., et al. (2012). Protein Arginine Methyltransferase 1-
771 directed Methylation of Kaposi Sarcoma-associated Herpesvirus Latency-associated Nuclear
772 Antigen*. J Biol Chem *287*, 5806–5818.

773 Carlomagno, Y., Zhang, Y., Davis, M., Lin, W.-L., Cook, C., Dunmore, J., Tay, W., Menkosky, K.,
774 Cao, X., Petrucelli, L., et al. (2014). Casein Kinase II Induced Polymerization of Soluble TDP-43
775 into Filaments Is Inhibited by Heat Shock Proteins. Plos One *9*, e90452.

776 Chang, C., Wu, T.-H., Wu, C.-Y., Chiang, M., Toh, E.K.-W., Hsu, Y.-C., Lin, K.-F., Liao, Y.,
777 Huang, T., and Huang, J.J.-T. (2012). The N-terminus of TDP-43 promotes its oligomerization and
778 enhances DNA binding affinity. Biochem Bioph Res Co *425*, 219–224.

779 Chang, Y.-I., Hsu, S.-C., Chau, G.-Y., Huang, C.-Y.F., Sung, J.-S., Hua, W.-K., and Lin, W.-J.
780 (2011). Identification of the methylation preference region in heterogeneous nuclear
781 ribonucleoprotein K by protein arginine methyltransferase 1 and its implication in regulating
782 nuclear/cytoplasmic distribution. Biochem Bioph Res Co *404*, 865–869.

783 Choksi, D.K., Roy, B., Chatterjee, S., Yusuff, T., Bakhoum, M.F., Sengupta, U., Ambegaokar, S.,
784 Kayed, R., and Jackson, G.R. (2014). TDP-43 Phosphorylation by casein kinase Iε promotes
785 oligomerization and enhances toxicity in vivo. Hum Mol Genet *23*, 1025–1035.

786 Conicella, A.E., Zerze, G.H., Mittal, J., and Fawzi, N.L. (2016). ALS Mutations Disrupt Phase
787 Separation Mediated by α-Helical Structure in the TDP-43 Low-Complexity C-Terminal Domain.
788 Structure *24*, 1537–1549.

789 Cook, C.N., Wu, Y., Odeh, H.M., Gendron, T.F., Jansen-West, K., Rosso, G. del, Yue, M., Jiang,
790 P., Gomes, E., Tong, J., et al. (2020). C9orf72 poly(GR) aggregation induces TDP-43
791 proteinopathy. Sci Transl Med *12*, eabb3774.

792 Corrêa, S.A.L., and Eales, K.L. (2012). The Role of p38 MAPK and Its Substrates in Neuronal
793 Plasticity and Neurodegenerative Disease. J Signal Transduct *2012*, 649079.

794 Cuadrado, A., and Nebreda, A.R. (2010). Mechanisms and functions of p38 MAPK signalling.
795 Biochem J *429*, 403–417.

bioRxiv preprint doi: https://doi.org/10.1101/2021.08.04.455154; this version posted August 4, 2021. The copyright holder for this preprint (which was not certified by peer review) is the author/funder. All rights reserved. No reuse allowed without permission.

796 Cuenda, A., Cohen, P., Buée-Scherrer, V., and Goedert, M. (1997). Activation of stress-activated
797 protein kinase-3 (SAPK3) by cytokines and cellular stresses is mediated via SAPKK3 (MKK6);
798 comparison of the specificities of SAPK3 and SAPK2 (RK/p38). Embo J *16*, 295–305.

799 Cupo, R., and Shorter, J. (2020). Expression and Purification of Recombinant Skd3 (Human ClpB)
800 Protein and Tobacco Etch Virus (TEV) Protease from Escherichia coli. Bio-Protocol *10*, e3858.

801 Dewil, M., Cruz, V.F. dela, Bosch, L.V.D., and Robberecht, W. (2007). Inhibition of p38 mitogen
802 activated protein kinase activation and mutant SOD1G93A-induced motor neuron death. Neurobiol
803 Dis *26*, 332–341.

804 Diskin, R., Askari, N., Capone, R., Engelberg, D., and Livnah, O. (2004). Active Mutants of the
805 Human p38α Mitogen-activated Protein Kinase*. J Biol Chem *279*, 47040–47049.

806 Duffy, J.P., Harrington, E.M., Salituro, F.G., Cochran, J.E., Green, J., Gao, H., Bemis, G.W.,
807 Evindar, G., Galullo, V.P., Ford, P.J., et al. (2011). The Discovery of VX-745: A Novel and
808 Selective p38α Kinase Inhibitor. Acs Med Chem Lett *2*, 758–763.

809 Eng, J.K., McCormack, A.L., and Yates, J.R. (1994). An approach to correlate tandem mass
810 spectral data of peptides with amino acid sequences in a protein database. J Am Soc Mass Spectr *5*,
811 976–989.

812 Freibaum, B.D., Chitta, R.K., High, A.A., and Taylor, J.P. (2010). Global Analysis of TDP-43
813 Interacting Proteins Reveals Strong Association with RNA Splicing and Translation Machinery. J
814 Proteome Res *9*, 1104–1120.

815 Gasset-Rosa, F., Lu, S., Yu, H., Chen, C., Melamed, Z., Guo, L., Shorter, J., Cruz, S.D., and
816 Cleveland, D.W. (2019). Cytoplasmic TDP-43 De-mixing Independent of Stress Granules Drives
817 Inhibition of Nuclear Import, Loss of Nuclear TDP-43, and Cell Death. Neuron *102*, 339-357.e7.

818 Germann, U.A., and Alam, J.J. (2020). P38α MAPK Signaling—A Robust Therapeutic Target for
819 Rab5-Mediated Neurodegenerative Disease. Int J Mol Sci *21*, 5485.

820 Gibbs, K.L., Kalmar, B., Rhymes, E.R., Fellows, A.D., Ahmed, M., Whiting, P., Davies, C.H.,
821 Greensmith, L., and Schiavo, G. (2018). Inhibiting p38 MAPK alpha rescues axonal retrograde
822 transport defects in a mouse model of ALS. Cell Death Dis *9*, 596.

823 Gitcho, M.A., Bigio, E.H., Mishra, M., Johnson, N., Weintraub, S., Mesulam, M., Rademakers, R.,
824 Chakraverty, S., Cruchaga, C., Morris, J.C., et al. (2009). TARDBP 3′-UTR variant in autopsy-
825 confirmed frontotemporal lobar degeneration with TDP-43 proteinopathy. Acta Neuropathol *118*,
826 633.

827 Goh, C.W., Lee, I.C., Sundaram, J.R., George, S.E., Yusoff, P., Brush, M.H., Sze, N.S.K., and
828 Shenolikar, S. (2018). Chronic oxidative stress promotes GADD34-mediated phosphorylation of the
829 TAR DNA-binding protein TDP-43, a modification linked to neurodegeneration. J Biol Chem *293*,
830 163–176.

831 Goldstein, D.M., Soth, M., Gabriel, T., Dewdney, N., Kuglstatter, A., Arzeno, H., Chen, J.,
832 Bingenheimer, W., Dalrymple, S.A., Dunn, J., et al. (2011). Discovery of 6-(2,4-Difluorophenoxy)-
833 2-[3-hydroxy-1-(2-hydroxyethyl)propylamino]-8-methyl-8 H -pyrido[2,3- d]pyrimidin-7-one

bioRxiv preprint doi: https://doi.org/10.1101/2021.08.04.455154; this version posted August 4, 2021. The copyright holder for this preprint (which was not certified by peer review) is the author/funder. All rights reserved. No reuse allowed without permission.

834 (Pamapimod) and 6-(2,4-Difluorophenoxy)-8-methyl-2-(tetrahydro-2 H -pyran-4-
835 ylamino)pyrido[2,3- d]pyrimidin-7(8 H)-one (R1487) as Orally Bioavailable and Highly Selective
836 Inhibitors of p38α Mitogen-Activated Protein Kinase. J Med Chem *54*, 2255–2265.

837 Guo, L., and Shorter, J. (2017). Biology and Pathobiology of TDP-43 and Emergent Therapeutic
838 Strategies. Csh Perspect Med *7*, a024554.

839 Guo, A., Gu, H., Zhou, J., Mulhern, D., Wang, Y., Lee, K.A., Yang, V., Aguiar, M., Kornhauser, J.,
840 Jia, X., et al. (2014). Immunoaffinity Enrichment and Mass Spectrometry Analysis of Protein
841 Methylation. Mol Cell Proteomics *13*, 372–387.

842 Guo, Z., Zheng, L., Xu, H., Dai, H., Zhou, M., Pascua, M.R., Chen, Q.M., and Shen, B. (2010).
843 Methylation of FEN1 suppresses nearby phosphorylation and facilitates PCNA binding. Nat Chem
844 Biol *6*, 766–773.

845 Harrison, A.F., and Shorter, J. (2017). RNA-binding proteins with prion-like domains in health and
846 disease. Biochem J *474*, 1417–1438.

847 Hasegawa, M., Arai, T., Nonaka, T., Kametani, F., Yoshida, M., Hashizume, Y., Beach, T.G.,
848 Buratti, E., Baralle, F., Morita, M., et al. (2008). Phosphorylated TDP-43 in frontotemporal lobar
849 degeneration and amyotrophic lateral sclerosis. Ann Neurol *64*, 60–70.

850 Hsu, J.-M., Chen, C.-T., Chou, C.-K., Kuo, H.-P., Li, L.-Y., Lin, C.-Y., Lee, H.-J., Wang, Y.-N.,
851 Liu, M., Liao, H.-W., et al. (2011). Crosstalk between Arg 1175 methylation and Tyr 1173
852 phosphorylation negatively modulates EGFR-mediated ERK activation. Nat Cell Biol *13*, 174–181.

853 Huang, L., Wang, Z., Narayanan, N., and Yang, Y. (2018). Arginine methylation of the C-terminus
854 RGG motif promotes TOP3B topoisomerase activity and stress granule localization. Nucleic Acids
855 Res *46*, gky103-.

856 Huq, M.D.M., Gupta, P., Tsai, N., White, R., Parker, M.G., and Wei, L. (2006). Suppression of
857 receptor interacting protein 140 repressive activity by protein arginine methylation. Embo J *25*,
858 5094–5104.

859 Jiang, L.-L., Xue, W., Hong, J.-Y., Zhang, J.-T., Li, M.-J., Yu, S.-N., He, J.-H., and Hu, H.-Y.
860 (2017). The N-terminal dimerization is required for TDP-43 splicing activity. Sci Rep-Uk *7*, 6196.

861 Johnson, B.S., Snead, D., Lee, J.J., McCaffery, J.M., Shorter, J., and Gitler, A.D. (2009). TDP-43 Is
862 Intrinsically Aggregation-prone, and Amyotrophic Lateral Sclerosis-linked Mutations Accelerate
863 Aggregation and Increase Toxicity*. J Biol Chem *284*, 20329–20339.

864 Kametani, F., Nonaka, T., Suzuki, T., Arai, T., Dohmae, N., Akiyama, H., and Hasegawa, M.
865 (2009). Identification of casein kinase-1 phosphorylation sites on TDP-43. Biochem Bioph Res Co
866 *382*, 405–409.

867 Kametani, F., Obi, T., Shishido, T., Akatsu, H., Murayama, S., Saito, Y., Yoshida, M., and
868 Hasegawa, M. (2016). Mass spectrometric analysis of accumulated TDP-43 in amyotrophic lateral
869 sclerosis brains. Sci Rep-Uk *6*, 23281.

bioRxiv preprint doi: https://doi.org/10.1101/2021.08.04.455154; this version posted August 4, 2021. The copyright holder for this preprint (which was not certified by peer review) is the author/funder. All rights reserved. No reuse allowed without permission.

870 Kawahara, Y., and Mieda-Sato, A. (2012). TDP-43 promotes microRNA biogenesis as a component
871 of the Drosha and Dicer complexes. Proc National Acad Sci *109*, 3347–3352.

872 Khalfallah, Y., Kuta, R., Grasmuck, C., Prat, A., Durham, H.D., and Velde, C.V. (2018). TDP-43
873 regulation of stress granule dynamics in neurodegenerative disease-relevant cell types. Sci Rep-Uk
874 *8*, 7551.

875 Kim, K.Y., Lee, H.-W., Shim, Y., Mook-Jung, I., Jeon, G.S., and Sung, J.-J. (2015). A
876 phosphomimetic mutant TDP-43 (S409/410E) induces Drosha instability and cytotoxicity in Neuro
877 2A cells. Biochem Bioph Res Co *464*, 236–243.

878 Lalmansingh, A.S., Urekar, C.J., and Reddi, P.P. (2011). TDP-43 Is a Transcriptional Repressor
879 THE TESTIS-SPECIFIC MOUSE acrv1 GENE IS A TDP-43 TARGET IN VIVO*. J Biol Chem
880 *286*, 10970–10982.

881 Larsen, S.C., Sylvestersen, K.B., Mund, A., Lyon, D., Mullari, M., Madsen, M.V., Daniel, J.A.,
882 Jensen, L.J., and Nielsen, M.L. (2016). Proteome-wide analysis of arginine monomethylation
883 reveals widespread occurrence in human cells. Sci Signal *9*, rs9–rs9.

884 Li, H.-R., Chen, T.-C., Hsiao, C.-L., Shi, L., Chou, C.-Y., and Huang, J. (2018). The physical forces
885 mediating self-association and phase-separation in the C-terminal domain of TDP-43. Biochimica
886 Et Biophysica Acta Bba - Proteins Proteom *1866*, 214–223.

887 Li, H.-Y., Yeh, P.-A., Chiu, H.-C., Tang, C.-Y., and Tu, B.P. (2011). Hyperphosphorylation as a
888 Defense Mechanism to Reduce TDP-43 Aggregation. Plos One *6*, e23075.

889 Liachko, N.F., Guthrie, C.R., and Kraemer, B.C. (2010). Phosphorylation Promotes Neurotoxicity
890 in a Caenorhabditis elegans Model of TDP-43 Proteinopathy. J Neurosci *30*, 16208–16219.

891 Liachko, N.F., McMillan, P.J., Guthrie, C.R., Bird, T.D., Leverenz, J.B., and Kraemer, B.C. (2013).
892 CDC7 inhibition blocks pathological TDP-43 phosphorylation and neurodegeneration. Ann Neurol
893 *74*, 39–52.

894 Liachko, N.F., McMillan, P.J., Strovas, T.J., Loomis, E., Greenup, L., Murrell, J.R., Ghetti, B.,
895 Raskind, M.A., Montine, T.J., Bird, T.D., et al. (2014). The Tau Tubulin Kinases TTBK1/2
896 Promote Accumulation of Pathological TDP-43. Plos Genet *10*, e1004803.

897 Ling, S.-C., Albuquerque, C.P., Han, J.S., Lagier-Tourenne, C., Tokunaga, S., Zhou, H., and
898 Cleveland, D.W. (2010). ALS-associated mutations in TDP-43 increase its stability and promote
899 TDP-43 complexes with FUS/TLS. Proc National Acad Sci *107*, 13318–13323.

900 Liu, L., Sun, W., Fan, X., Xu, Y., Cheng, M., and Zhang, Y. (2019). Methylation of C/EBPα by
901 PRMT1 inhibits its tumor suppressive function in breast cancer. Cancer Res *79*, canres.3211.2018.

902 Liu, Y.-J., Ju, T.-C., Chen, H.-M., Jang, Y.-S., Lee, L.-M., Lai, H.-L., Tai, H.-C., Fang, J.-M., Lin,
903 Y.-L., Tu, P.-H., et al. (2015). Activation of AMP-activated protein kinase α1 mediates
904 mislocalization of TDP-43 in amyotrophic lateral sclerosis. Hum Mol Genet *24*, 787–801.

bioRxiv preprint doi: https://doi.org/10.1101/2021.08.04.455154; this version posted August 4, 2021. The copyright holder for this preprint (which was not certified by peer review) is the author/funder. All rights reserved. No reuse allowed without permission.

905 Lu, Y., Ma, W., Li, Z., Lu, J., and Wang, X. (2017). The interplay between p16 serine
906 phosphorylation and arginine methylation determines its function in modulating cellular apoptosis
907 and senescence. Sci Rep-Uk *7*, 41390.

908 Mann, J.R., Gleixner, A.M., Mauna, J.C., Gomes, E., DeChellis-Marks, M.R., Needham, P.G.,
909 Copley, K.E., Hurtle, B., Portz, B., Pyles, N.J., et al. (2019). RNA Binding Antagonizes Neurotoxic
910 Phase Transitions of TDP-43. Neuron *102*, 321-338.e8.

911 McDonald, K.K., Aulas, A., Destroismaisons, L., Pickles, S., Beleac, E., Camu, W., Rouleau, G.A.,
912 and Velde, C.V. (2011). TAR DNA-binding protein 43 (TDP-43) regulates stress granule dynamics
913 via differential regulation of G3BP and TIA-1. Hum Mol Genet *20*, 1400–1410.

914 McGurk, L., Gomes, E., Guo, L., Mojsilovic-Petrovic, J., Tran, V., Kalb, R.G., Shorter, J., and
915 Bonini, N.M. (2018). Poly(ADP-Ribose) Prevents Pathological Phase Separation of TDP-43 by
916 Promoting Liquid Demixing and Stress Granule Localization. Mol Cell *71*, 703-717.e9.

917 Meyerowitz, J., Parker, S.J., Vella, L.J., Ng, D.C., Price, K.A., Liddell, J.R., Caragounis, A., Li, Q.-
918 X., Masters, C.L., Nonaka, T., et al. (2011). C-Jun N-terminal kinase controls TDP-43 accumulation
919 in stress granules induced by oxidative stress. Mol Neurodegener *6*, 57.

920 Molliex, A., Temirov, J., Lee, J., Coughlin, M., Kanagaraj, A.P., Kim, H.J., Mittag, T., and Taylor,
921 J.P. (2015). Phase Separation by Low Complexity Domains Promotes Stress Granule Assembly and
922 Drives Pathological Fibrillization. Cell *163*, 123–133.

923 Morrison, D.K. (2012). MAP Kinase Pathways. Csh Perspect Biol *4*, a011254.

924 Neumann, M., Sampathu, D.M., Kwong, L.K., Truax, A.C., Micsenyi, M.C., Chou, T.T., Bruce, J.,
925 Schuck, T., Grossman, M., Clark, C.M., et al. (2006). Ubiquitinated TDP-43 in Frontotemporal
926 Lobar Degeneration and Amyotrophic Lateral Sclerosis. Science *314*, 130–133.

927 Neumann, M., Kwong, L.K., Lee, E.B., Kremmer, E., Flatley, A., Xu, Y., Forman, M.S., Troost, D.,
928 Kretzschmar, H.A., Trojanowski, J.Q., et al. (2009). Phosphorylation of S409/410 of TDP-43 is a
929 consistent feature in all sporadic and familial forms of TDP-43 proteinopathies. Acta Neuropathol
930 *117*, 137–149.

931 Nguyen, H.P., Broeckhoven, C.V., and Zee, J. van der (2018). ALS Genes in the Genomic Era and
932 their Implications for FTD. Trends Genet *34*, 404–423.

933 Nonaka, T., Arai, T., Buratti, E., Baralle, F.E., Akiyama, H., and Hasegawa, M. (2009).
934 Phosphorylated and ubiquitinated TDP-43 pathological inclusions in ALS and FTLD-U are
935 recapitulated in SH-SY5Y cells. Febs Lett *583*, 394–400.

936 Nonaka, T., Suzuki, G., Tanaka, Y., Kametani, F., Hirai, S., Okado, H., Miyashita, T., Saitoe, M.,
937 Akiyama, H., Masai, H., et al. (2016). Phosphorylation of TAR DNA-binding Protein of 43 kDa
938 (TDP-43) by Truncated Casein Kinase 1δ Triggers Mislocalization and Accumulation of TDP-43*.
939 J Biol Chem *291*, 5473–5483.

940 Ortega, J.A., Daley, E.L., Kour, S., Samani, M., Tellez, L., Smith, H.S., Hall, E.A., Esengul, Y.T.,
941 Tsai, Y.-H., Gendron, T.F., et al. (2020). Nucleocytoplasmic Proteomic Analysis Uncovers eRF1

bioRxiv preprint doi: https://doi.org/10.1101/2021.08.04.455154; this version posted August 4, 2021. The copyright holder for this preprint (which was not certified by peer review) is the author/funder. All rights reserved. No reuse allowed without permission.

942 and Nonsense-Mediated Decay as Modifiers of ALS/FTD C9orf72 Toxicity. Neuron *106*, 90-
943 107.e13.

944 Peng, J., and Gygi, S.P. (2001). Proteomics: the move to mixtures. J Mass Spectrom *36*, 1083–
945 1091.

946 Pickhardt, M., Tassoni, M., Denner, P., Kurkowsky, B., Kitanovic, A., Möhl, C., Fava, E., and
947 Mandelkow, E. (2019). Screening of a neuronal cell model of tau pathology for therapeutic
948 compounds. Neurobiol Aging *76*, 24–34.

949 Polymenidou, M., Lagier-Tourenne, C., Hutt, K.R., Huelga, S.C., Moran, J., Liang, T.Y., Ling, S.-
950 C., Sun, E., Wancewicz, E., Mazur, C., et al. (2011). Long pre-mRNA depletion and RNA
951 missplicing contribute to neuronal vulnerability from loss of TDP-43. Nat Neurosci *14*, 459–468.

952 Portz, B., Lee, B.L., and Shorter, J. (2021). FUS and TDP-43 Phases in Health and Disease. Trends
953 Biochem Sci *46*, 550–563.

954 Prasad, A., Bharathi, V., Sivalingam, V., Girdhar, A., and Patel, B.K. (2019). Molecular
955 Mechanisms of TDP-43 Misfolding and Pathology in Amyotrophic Lateral Sclerosis. Front Mol
956 Neurosci *12*, 25.

957 Prins, N.D., Harrison, J.E., Chu, H.-M., Blackburn, K., Alam, J.J., Scheltens, P., Arnold, Coskinas,
958 Gonzales, Joseph, et al. (2021). A phase 2 double-blind placebo-controlled 24-week treatment
959 clinical study of the p38 alpha kinase inhibitor neflamapimod in mild Alzheimer's disease.
960 Alzheimer's Res Ther *13*, 106.

961 Qamar, S., Wang, G., Randle, S.J., Ruggeri, F.S., Varela, J.A., Lin, J.Q., Phillips, E.C., Miyashita,
962 A., Williams, D., Ströhl, F., et al. (2018). FUS Phase Separation Is Modulated by a Molecular
963 Chaperone and Methylation of Arginine Cation-π Interactions. Cell *173*, 720-734.e15.

964 Ratovitski, T., Arbez, N., Stewart, J.C., Chighladze, E., and Ross, C.A. (2015). PRMT5- mediated
965 symmetric arginine dimethylation is attenuated by mutant huntingtin and is impaired in
966 Huntington's disease (HD). Cell Cycle *14*, 1716–1729.

967 Rowland, L.P., and Shneider, N.A. (2001). Amyotrophic Lateral Sclerosis. New Engl J Medicine
968 *344*, 1688–1700.

969 Shevchenko, A., Wilm, M., Vorm, O., and Mann, M. (1996). Mass Spectrometric Sequencing of
970 Proteins from Silver-Stained Polyacrylamide Gels. Anal Chem *68*, 850–858.

971 Silva, L.G. da, Simonetti, F., Hutten, S., Riemenschneider, H., Sternburg, E.L., Pietrek, L.M.,
972 Gebel, J., Dötsch, V., Edbauer, D., Hummer, G., et al. (2021). Disease-linked TDP-43
973 hyperphosphorylation suppresses TDP-43 condensation and aggregation. Biorxiv
974 2021.04.30.442163.

975 Simandi, Z., Pajer, K., Karolyi, K., Sieler, T., Jiang, L.-L., Kolostyak, Z., Sari, Z., Fekecs, Z., Pap,
976 A., Patsalos, A., et al. (2018). Arginine Methyltransferase PRMT8 Provides Cellular Stress
977 Tolerance in Aging Motoneurons. J Neurosci *38*, 7683–7700.

bioRxiv preprint doi: https://doi.org/10.1101/2021.08.04.455154; this version posted August 4, 2021. The copyright holder for this preprint (which was not certified by peer review) is the author/funder. All rights reserved. No reuse allowed without permission.

978 Sreedharan, J., Blair, I.P., Tripathi, V.B., Hu, X., Vance, C., Rogelj, B., Ackerley, S., Durnall, J.C.,
979 Williams, K.L., Buratti, E., et al. (2008). TDP-43 Mutations in Familial and Sporadic Amyotrophic
980 Lateral Sclerosis. Science *319*, 1668–1672.

981 Sreedharan, J., Neukomm, L.J., Brown, R.H., and Freeman, M.R. (2015). Age-Dependent TDP-43-
982 Mediated Motor Neuron Degeneration Requires GSK3, hat-trick, and xmas-2. Curr Biol *25*, 2130–
983 2136.

984 Tang, J., Frankel, A., Cook, R.J., Kim, S., Paik, W.K., Williams, K.R., Clarke, S., and Herschman,
985 H.R. (2000). PRMT1 Is the Predominant Type I Protein Arginine Methyltransferase in Mammalian
986 Cells*. J Biol Chem *275*, 7723–7730.

987 Taylor, L.M., McMillan, P.J., Liachko, N.F., Strovas, T.J., Ghetti, B., Bird, T.D., Keene, C.D., and
988 Kraemer, B.C. (2018). Pathological phosphorylation of tau and TDP-43 by TTBK1 and TTBK2
989 drives neurodegeneration. Mol Neurodegener *13*, 7.

990 Thandapani, P., O'Connor, T.R., Bailey, T.L., and Richard, S. (2013). Defining the RGG/RG Motif.
991 Mol Cell *50*, 613–623.

992 Tollervey, J.R., Curk, T., Rogelj, B., Briese, M., Cereda, M., Kayikci, M., König, J., Hortobágyi,
993 T., Nishimura, A.L., Župunski, V., et al. (2011). Characterizing the RNA targets and position-
994 dependent splicing regulation by TDP-43. Nat Neurosci *14*, 452–458.

995 Tortarolo, M., Veglianese, P., Calvaresi, N., Botturi, A., Rossi, C., Giorgini, A., Migheli, A., and
996 Bendotti, C. (2003). Persistent activation of p38 mitogen-activated protein kinase in a mouse model
997 of familial amyotrophic lateral sclerosis correlates with disease progression. Mol Cell Neurosci *23*,
998 180–192.

999 Valdmanis, P.N., and Rouleau, G.A. (2008). Genetics of familial amyotrophic lateral sclerosis.
1000 Neurology *70*, 144–152.

1001 Wall, M.L., and Lewis, S.M. (2017). Methylarginines within the RGG-Motif Region of hnRNP A1
1002 Affect Its IRES Trans-Acting Factor Activity and Are Required for hnRNP A1 Stress Granule
1003 Localization and Formation. J Mol Biol *429*, 295–307.

1004 Wang, A., Conicella, A.E., Schmidt, H.B., Martin, E.W., Rhoads, S.N., Reeb, A.N., Nourse, A.,
1005 Montero, D.R., Ryan, V.H., Rohatgi, R., et al. (2018). A single N-terminal phosphomimic disrupts
1006 TDP-43 polymerization, phase separation, and RNA splicing. Embo J *37*.

1007 Watkins, J., Ghosh, A., Keerie, A.F.A., Alix, J.J.P., Mead, R.J., and Sreedharan, J. (2020). Female
1008 sex mitigates motor and behavioural phenotypes in TDP-43Q331K knock-in mice. Sci Rep-Uk *10*,
1009 19220.

1010 Winton, M.J., Igaz, L.M., Wong, M.M., Kwong, L.K., Trojanowski, J.Q., and Lee, V.M.-Y. (2008).
1011 Disturbance of Nuclear and Cytoplasmic TAR DNA-binding Protein (TDP-43) Induces Disease-
1012 like Redistribution, Sequestration, and Aggregate Formation*. J Biol Chem *283*, 13302–13309.

1013 Winzen, R., Kracht, M., Ritter, B., Wilhelm, A., Chen, C.A., Shyu, A., Müller, M., Gaestel, M.,
1014 Resch, K., and Holtmann, H. (1999). The p38 MAP kinase pathway signals for cytokine-induced

bioRxiv preprint doi: https://doi.org/10.1101/2021.08.04.455154; this version posted August 4, 2021. The copyright holder for this preprint (which was not certified by peer review) is the author/funder. All rights reserved. No reuse allowed without permission.

1015 mRNA stabilization via MAP kinase-activated protein kinase 2 and an AU-rich region-targeted
1016 mechanism. Embo J *18*, 4969–4980.

1017 Wobst, H.J., Wesolowski, S.S., Chadchankar, J., Delsing, L., Jacobsen, S., Mukherjee, J., Deeb,
1018 T.Z., Dunlop, J., Brandon, N.J., and Moss, S.J. (2017). Cytoplasmic Relocalization of TAR DNA-
1019 Binding Protein 43 Is Not Sufficient to Reproduce Cellular Pathologies Associated with ALS In
1020 vitro. Frontiers in Molecular Neuroscience *10*, 46.

1021 Wobst, H.J., Mack, K.L., Brown, D.G., Brandon, N.J., and Shorter, J. (2020). The clinical trial
1022 landscape in amyotrophic lateral sclerosis—Past, present, and future. Med Res Rev *40*, 1352–1384.

1023 Xiong, H.-L., Wang, J.-Y., Sun, Y.-M., Wu, J.-J., Chen, Y., Qiao, K., Zheng, Q.-J., Zhao, G., and
1024 Wu, Z.-Y. (2010). Association between novel TARDBP mutations and Chinese patients with
1025 amyotrophic lateral sclerosis. Bmc Med Genet *11*, 8.

1026 Xu, Y.-F., Zhang, Y.-J., Lin, W.-L., Cao, X., Stetler, C., Dickson, D.W., Lewis, J., and Petrucelli,
1027 L. (2011). Expression of mutant TDP-43 induces neuronal dysfunction in transgenic mice. Mol
1028 Neurodegener *6*, 73.

1029 Yamagata, K., Daitoku, H., Takahashi, Y., Namiki, K., Hisatake, K., Kako, K., Mukai, H., Kasuya,
1030 Y., and Fukamizu, A. (2008). Arginine Methylation of FOXO Transcription Factors Inhibits Their
1031 Phosphorylation by Akt. Mol Cell *32*, 221–231.

1032 Yasuda, S., Sugiura, H., Tanaka, H., Takigami, S., and Yamagata, K. (2011). p38 MAP Kinase
1033 Inhibitors as Potential Therapeutic Drugs for Neural Diseases. Central Nerv Syst Agents Medicinal
1034 Chem *11*, 45–59.

1035 Zarubin, T., and Han, J. (2005). Activation and signaling of the p38 MAP kinase pathway. Cell Res
1036 *15*, 11–18.

1037 Zhan, L., Xie, Q., and Tibbetts, R.S. (2015). Opposing roles of p38 and JNK in a Drosophila model
1038 of TDP-43 proteinopathy reveal oxidative stress and innate immunity as pathogenic components of
1039 neurodegeneration. Hum Mol Genet *24*, 757–772.

1040 Zhang, Y.-J., Gendron, T.F., Xu, Y.-F., Ko, L.-W., Yen, S.-H., and Petrucelli, L. (2010).
1041 Phosphorylation regulates proteasomal-mediated degradation and solubility of TAR DNA binding
1042 protein-43 C-terminal fragments. Mol Neurodegener *5*, 33.

1043 Zou, Z.-Y., Peng, Y., Wang, X.-N., Liu, M.-S., Li, X.-G., and Cui, L.-Y. (2012). Screening of the
1044 TARDBP gene in familial and sporadic amyotrophic lateral sclerosis patients of Chinese origin.
1045 Neurobiol Aging *33*, 2229.e11-2229.e18.

1046

bioRxiv preprint doi: https://doi.org/10.1101/2021.08.04.455154; this version posted August 4, 2021. The copyright holder for this preprint (which was not certified by peer review) is the author/funder. All rights reserved. No reuse allowed without permission.

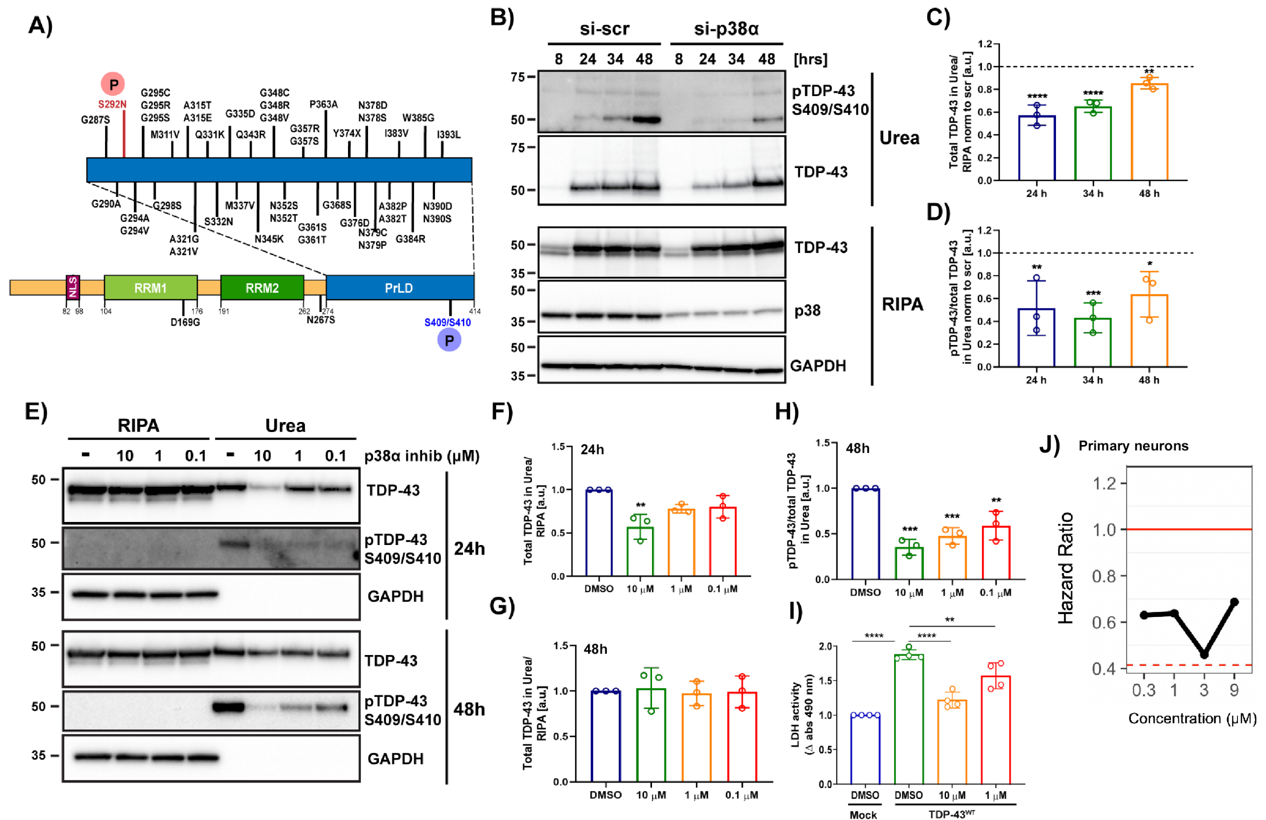

1047

1048 **Figure 1. Genetic and pharmacological inhibition of p38α MAPK reduces TDP-43 aggregation**
1049 **and phosphorylation at S409/S410, and inhibits TDP-43-induced neurotoxicity. A)** Schematic of
1050 domain architecture of TDP-43 and location of ALS-linked mutations and phosphorylation sites (P)
1051 detected after p38α MAPK treatment *in vitro*. **B)** Western blot of total and phosphorylated TDP-
1052 43^{M337V} in RIPA and urea fractions of SH-SY5Y cells with siRNA-induced p38α knockdown.
1053 GAPDH was used as a loading control. **C)** Quantification of urea/RIPA ratio of total TDP-43
1054 normalized to levels in scrambled siRNA (si-scr). **D)** Quantification of pTDP-43/total TDP-43 ratio
1055 in urea fraction normalized to levels in si-scr (mean band signal ± SD, two-way ANOVA with Sidak's
1056 multiple comparison test, n = 3). **E)** Western blot of total and pTDP-43^{M337V} in RIPA and urea
1057 fractions of SH-SY5Y cells with pharmacological p38α inhibition with compound 1. GAPDH was
1058 used as a loading control. Quantification of urea/RIPA ratio of total TDP-43 at time points 24h **(F)**
1059 and 48h **(G)** post-transfection, and pTDP-43/total TDP-43 ratio in urea fraction at time point 48h
1060 post-transfection **(H)** normalized to levels in DMSO-treated cells (mean band signal ± SD, one-way
1061 ANOVA with Dunnett's multiple comparison test, n = 3). **I)** Quantification of LDH activity in
1062 conditioned medium normalized to levels in DMSO-treated TDP-43^{WT} -transfected NSC-34 cells.
1063 (one-way ANOVA with Dunnett's multiple comparison test, n = 4 with 6 replicates in each). $^{*}p <$
1064 0.05, $^{**}p < 0.01$ $^{***}p < 0.001$, $^{****}p < 0.0001$. **J)** Hazard ratios of primary neurons expressing mApple
1065 and TDP-43^{M337V}-EGFP treated with p38α inhibitor VX-745 at 0.3, 1, 3, and 9 μM compared with
1066 DMSO control (reference, set at 1.0) were 0.6296, 0.6378, 0.4596, and 0.6869 respectively.
1067 Reduction of hazard ratio was most significant at 3 μM (Cox proportional hazard, p<0.01).
1068 See also Figure S1.
1069

bioRxiv preprint doi: https://doi.org/10.1101/2021.08.04.455154; this version posted August 4, 2021. The copyright holder for this preprint (which was not certified by peer review) is the author/funder. All rights reserved. No reuse allowed without permission.

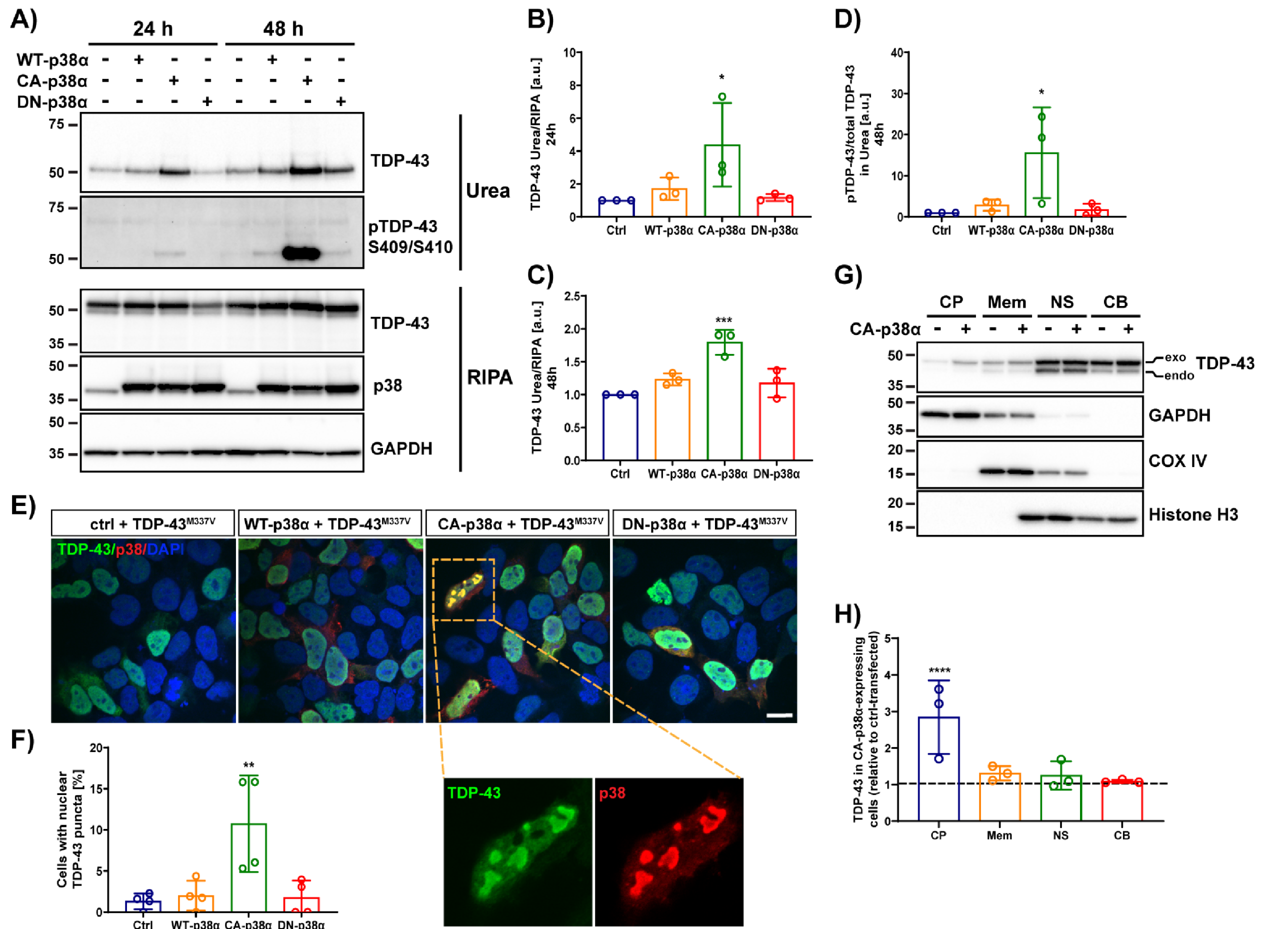

Figure 2. Constitutively active p38α induces aggregation, phosphorylation and cytoplasmic accumulation of TDP-43. A) Western blot of total and pTDP-43 in RIPA and urea fractions of SH-SY5Y cells co-transfected with TDP-43^{M337V} and empty control plasmid (Ctrl), WT-p38α, CA-p38α or DN-p38α. GAPDH was used as a loading control. Quantification of urea/RIPA ratio of total TDP-43 at time points 24h **(B)** or 48h **(C)** post-transfection, and pTDP-43/total TDP-43 ratio in urea fraction at time point 48h post-transfection **(D)**, normalized to levels in ctrl-plasmid transfected cells (mean band signal ± SD, one-way ANOVA with Dunnett's multiple comparison test, n = 3). **E)** Representative confocal images of SH-SY5Y cells co-expressing TDP-43^{M337V} (green) and WT-p38α, CA-p38α or DN-p38α (red) with quantification of the number of cells with nuclear TDP-43 puncta/granules **(F)** (one-way ANOVA with Dunnett's multiple comparison test, n = 4 and 10 fields each, scale bar 20 µm). **G)** Western blot of TDP-43 in different cellular compartments of SH-SY5Y cells co-transfected with TDP-43^{M337V} and ctrl-plasmid or CA-p38α. Exo denotes exogenous TDP-43 and endo denotes endogenous TDP-43. GAPDH was used as a loading control for cytoplasmic fraction (CP), COX IV for the membrane fraction (Mem), and histone H3 for the soluble nuclear (NS) and chromatin-bound (CB) fractions. **H)** Quantification of total TDP-43 in cytoplasmic, membrane, soluble nuclear and chromatin-bound fractions (mean band signal ± SD, two-way ANOVA with Sidak's multiple comparison test, n = 3). *$p < 0.05$, **$p < 0.01$ ***$p < 0.001$, ****$p < 0.0001$.

bioRxiv preprint doi: https://doi.org/10.1101/2021.08.04.455154; this version posted August 4, 2021. The copyright holder for this preprint (which was not certified by peer review) is the author/funder. All rights reserved. No reuse allowed without permission.

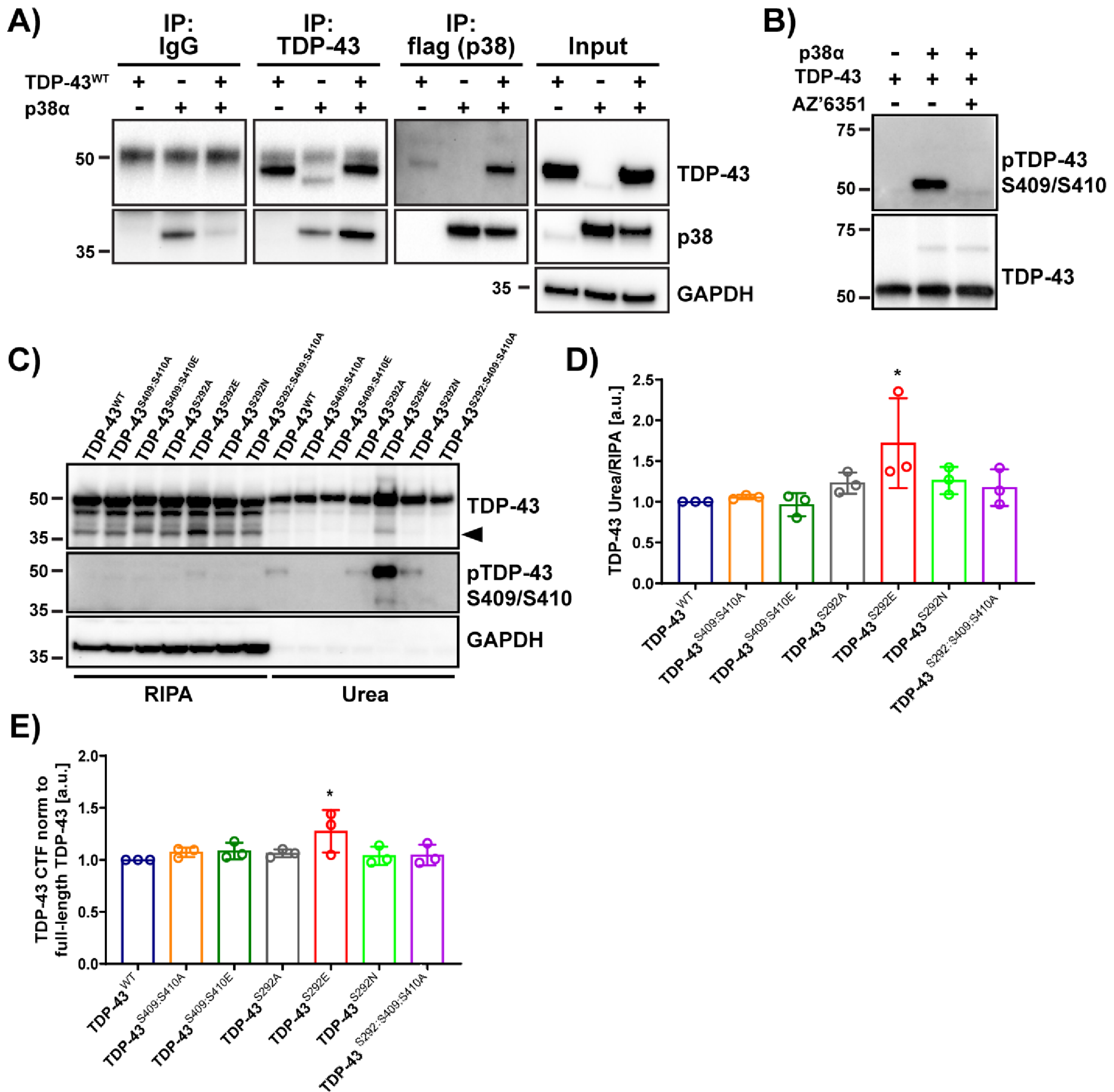

Figure 3. TDP-43 directly interacts with and is phosphorylated by p38α at S292 and S409/S410, with S292 regulating phosphorylation at S409/S410. A) Western blot of immunoprecipitated TDP-43^{WT} and co-immunoprecipitated WT-p38α and immunoprecipitated WT-p38α and co-immunoprecipitated TDP-43^{WT} in SH-SY5Y cells. Inputs are shown on the right. GAPDH was used as a loading control. **B)** Western blot of *in vitro* kinase assay (30°C for 30 min) of recombinant human TDP-43 (750 ng) and recombinant active p38α (300 ng) with and without the p38α inhibitor compound 1. **C)** Western blot of total and pTDP-43 in RIPA and urea fractions of SH-SY5Y cells transfected with TDP-43^{WT} and with S292 and S409/S410 mutant constructs. Quantification of urea/RIPA ratio of total TDP-43 **(D)**, and CTF/full length ratio of TDP-43 in RIPA fraction **(E)** at time point 24h post-transfection normalized to levels in TDP-43^{WT} (mean band signal ± SD, one-way ANOVA with Dunnett's multiple comparison test, n = 3). *$p < 0.05$.
See also Figure S2.

bioRxiv preprint doi: https://doi.org/10.1101/2021.08.04.455154; this version posted August 4, 2021. The copyright holder for this preprint (which was not certified by peer review) is the author/funder. All rights reserved. No reuse allowed without permission.

A)

Homo sapiens	287-GGFGN**SR**GGGAGLGNNQGSNMGGG-310
Pongo abelii	287-GGFGN**SR**GGGAGLGNNQGSNMGGG-310
Bos taurus	287-GGFGN**SR**GGGAGLGNNQGSNMGGG-310
Mus musculus	287-GGFGN**SR**GGGAGLGNNQGGNMGGG-310
Gallus gallus	287-GGFGN**SR**GGGGGLGNNQGSNMGGG-310

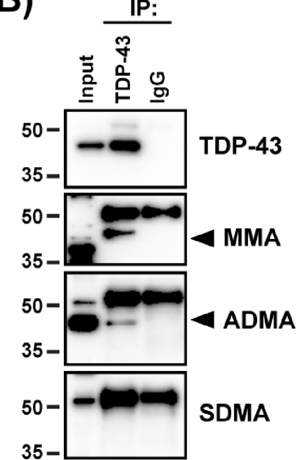

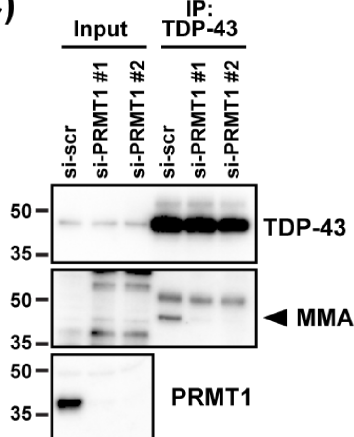

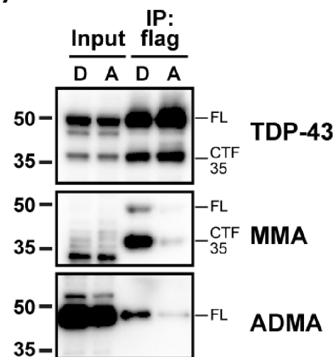

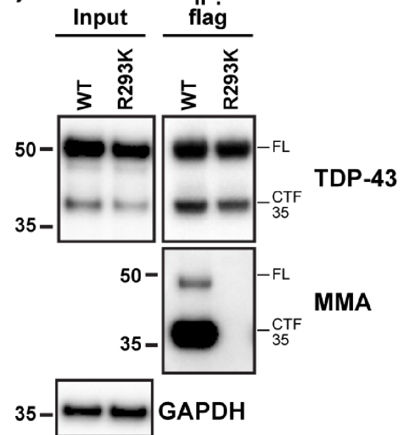

1103

1104 **Figure 4. TDP-43 is methylated by PRMT1 primarily at residue R293. A)** Sequence alignment
1105 of amino acids 287-310 of TDP-43 from diverse vertebrate species. Conserved S292 and R293 sites
1106 are bolded. S292 phosphorylation site and R293-G295 RGG-motif are highlighted in yellow and
1107 green, respectively. **B)** Western blot of immunoprecipitated endogenous TDP-43 from SH-SY5Y-
1108 cells probed with antibodies against TDP-43, ADMA, MMA and SDMA. TDP-43 with arginine
1109 methylation is marked by arrows. **C)** Western blot of immunoprecipitated endogenous TDP-43 from
1110 SH-SY5Y-cells with siRNA-induced PRMT1 knockdown probed with antibodies against TDP-43,
1111 MMA and PRMT1. **D)** Western blot of expressed and immunoprecipitated TDP-43^{WT} using anti-Flag
1112 antibody from SH-SY5Y-cells treated with DMSO (D) or with methyltransferase inhibitor AdOx (A)
1113 at a final concentration of 20 µM for 24h. FL denotes full-length TDP-43 and CTF35 denotes C-
1114 terminal 35kDa fragment of TDP-43. **E)** Western blot of expressed and immunoprecipitated TDP-
1115 43^{WT} and TDP-43^{R293K} using anti-Flag antibody from SH-SY5Y cells probed with antibodies against
1116 TDP-43 and MMA.
1117

1118

bioRxiv preprint doi: https://doi.org/10.1101/2021.08.04.455154; this version posted August 4, 2021. The copyright holder for this preprint (which was not certified by peer review) is the author/funder. All rights reserved. No reuse allowed without permission.

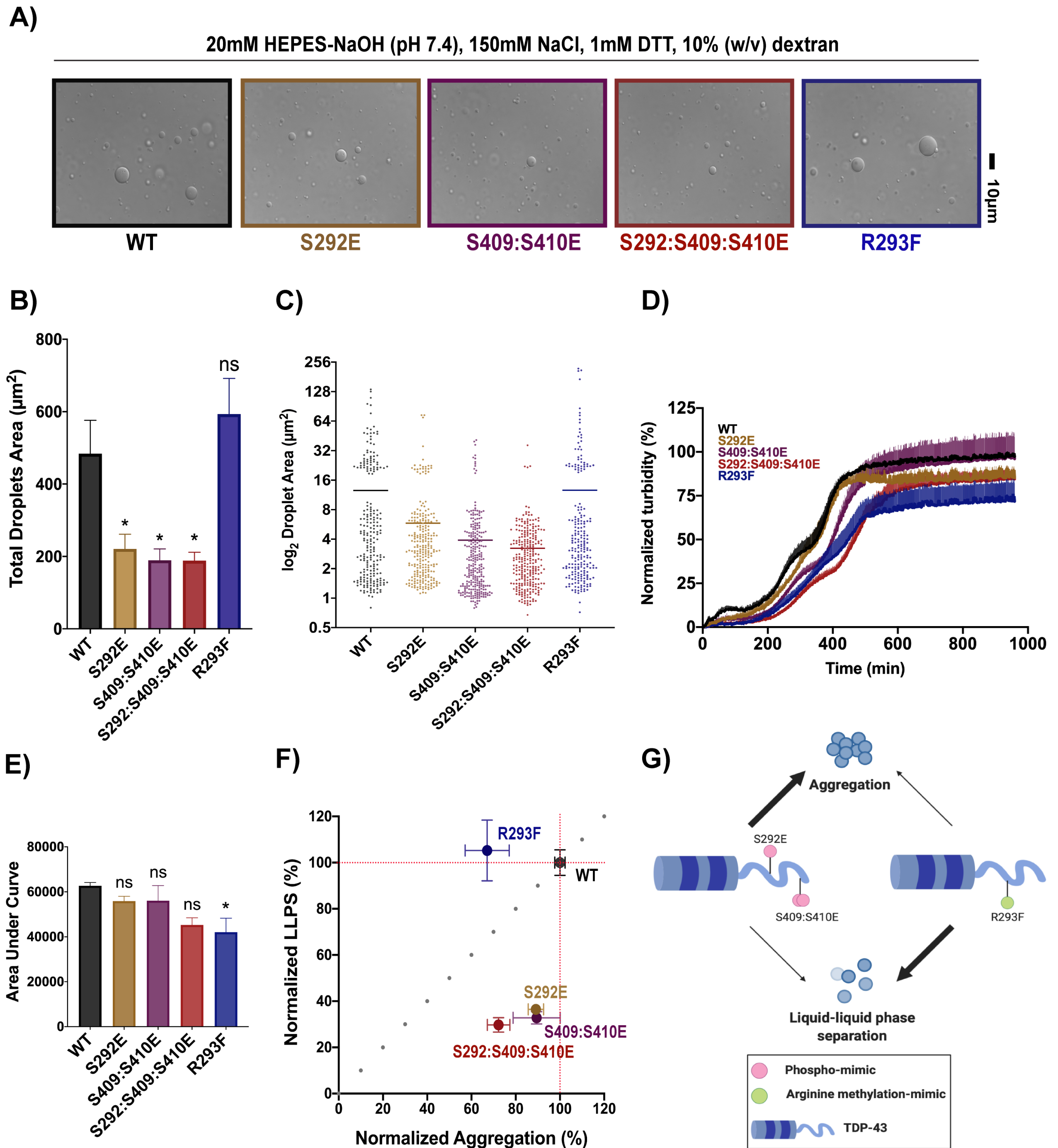

1119

1120 **Figure 5. TDP-43 phosphorylation favors aggregation whereas arginine methylation favors**
1121 **LLPS *in vitro*. A)** Representative DIC microscopy images of liquid-like droplets of 10µM TDP-43-
1122 MBP wild-type protein and its mutant forms. Purified recombinant proteins were incubated for 30
1123 minutes with phase separation buffer prior to imaging. Scale bar = 10 µm (n=3). **B)** Bar graph
1124 showing the total droplets area for each protein. Mean± SEM, one-way ANOVA with Dunnett's
1125 multiple comparison test (n=3, *p<0.05). **C)** Vertical scatterplot displaying the size distribution of
1126 droplets for each protein. Each data point corresponds to a single droplet. Bolded bars represent the
1127 average droplet area for each variant. **D)** Turbidity measurements of 5 µM TDP-43-MBP co-
1128 incubated with TEV protease (1 µg/mL). Turbidity was measured at an absorbance of 395 nm. Values
1129 represent the normalized mean ± SEM (n = 4). **E)** Aggregation data from **D** was quantified by
1130 calculating the area under the curve.Values represent means ± SEM (n = 4). One-way ANOVA with

bioRxiv preprint doi: https://doi.org/10.1101/2021.08.04.455154; this version posted August 4, 2021. The copyright holder for this preprint (which was not certified by peer review) is the author/funder. All rights reserved. No reuse allowed without permission.

1131 Tukey's multiple comparison test was performed (*$p<0.05$). **F)** LLPS versus aggregation plot shows
1132 the phospho-mimetics cluster below the y=x dotted line, whereas the arginine methylation-mimic
1133 appears above the y=x dotted line. Phospho-mimetics inhibit TDP-43 LLPS more severely than TDP-
1134 43 aggregation, whereas the arginine-methylation mimic inhibits TDP-43 aggregation but not TDP-
1135 43 LLPS. Y-axis represents normalized LLPS propensity relative to wild-type based on the average
1136 area of droplets from analysis in **C**. X-axis represents normalized aggregation relative to wild-type
1137 from **D**. Error bars represent SEM with n=3 for their respective dimension. **G)** Schematic diagram
1138 describing the dichotomy in outcomes between p38α-mediated TDP-43 phosphorylation and
1139 PRMT1-mediated arginine methylation. Phospho-mimicking mutants favor aberrant aggregation
1140 (thick arrow) over LLPS (thin arrow), whereas the arginine methylation-mimic favors LLPS (thick
1141 arrow) over aberrant aggregation (thin arrow). This panel was made with BioRender.
1142

bioRxiv preprint doi: https://doi.org/10.1101/2021.08.04.455154; this version posted August 4, 2021. The copyright holder for this preprint (which was not certified by peer review) is the author/funder. All rights reserved. No reuse allowed without permission.

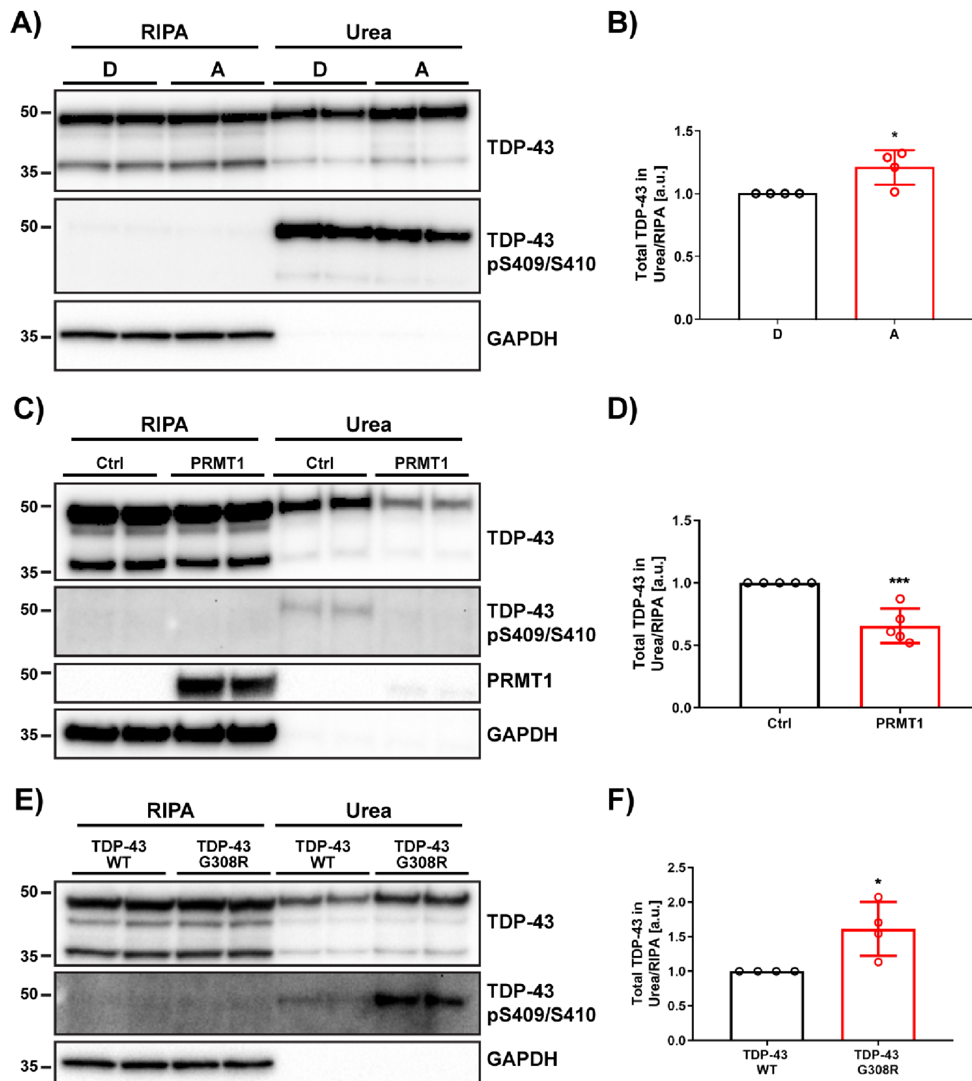

1143

1144 **Figure 6. Methylation of TDP-43 regulates its aggregation. A)** Western blot of total and pTDP-43
1145 in RIPA and urea fractions of TDP-43^{WT}-transfected SH-SY5Y-cells treated with DMSO (D) or with
1146 methyltransferase inhibitor AdOx (A) at a final concentration of 20 µM for 24h. **B)** Quantification of
1147 urea/RIPA ratio of total TDP-43 normalized to levels in DMSO-treated cells (mean band signal ± SD,
1148 unpaired t test, n = 4). **C)** Western blot of total and pTDP-43 in RIPA and urea fractions of TDP-
1149 43^{WT}-transfected SH-SY5Y-cells co-transfected with empty control plasmid (Ctrl) or PRMT1. **D)**
1150 Quantification of urea/RIPA ratio of total TDP-43 normalized to levels in Ctrl-plasmid co-transfected
1151 cells (mean band signal ± SD, unpaired t test, n = 5). **E)** Western blot of total and pTDP-43 in RIPA
1152 and urea fractions of TDP-43^{WT} or TDP-43^{G308R} transfected SH-SY5Y-cells at time point of 24h
1153 post-transfection. **F)** Quantification of urea/RIPA ratio of total TDP-43 normalized to levels in TDP-
1154 43^{WT}-transfected cells (mean band signal ± SD, one-way ANOVA with Dunnett's multiple
1155 comparison test, n = 4). $^{*}p < 0.05$, $^{***}p < 0.001$.
1156

bioRxiv preprint doi: https://doi.org/10.1101/2021.08.04.455154; this version posted August 4, 2021. The copyright holder for this preprint (which was not certified by peer review) is the author/funder. All rights reserved. No reuse allowed without permission.

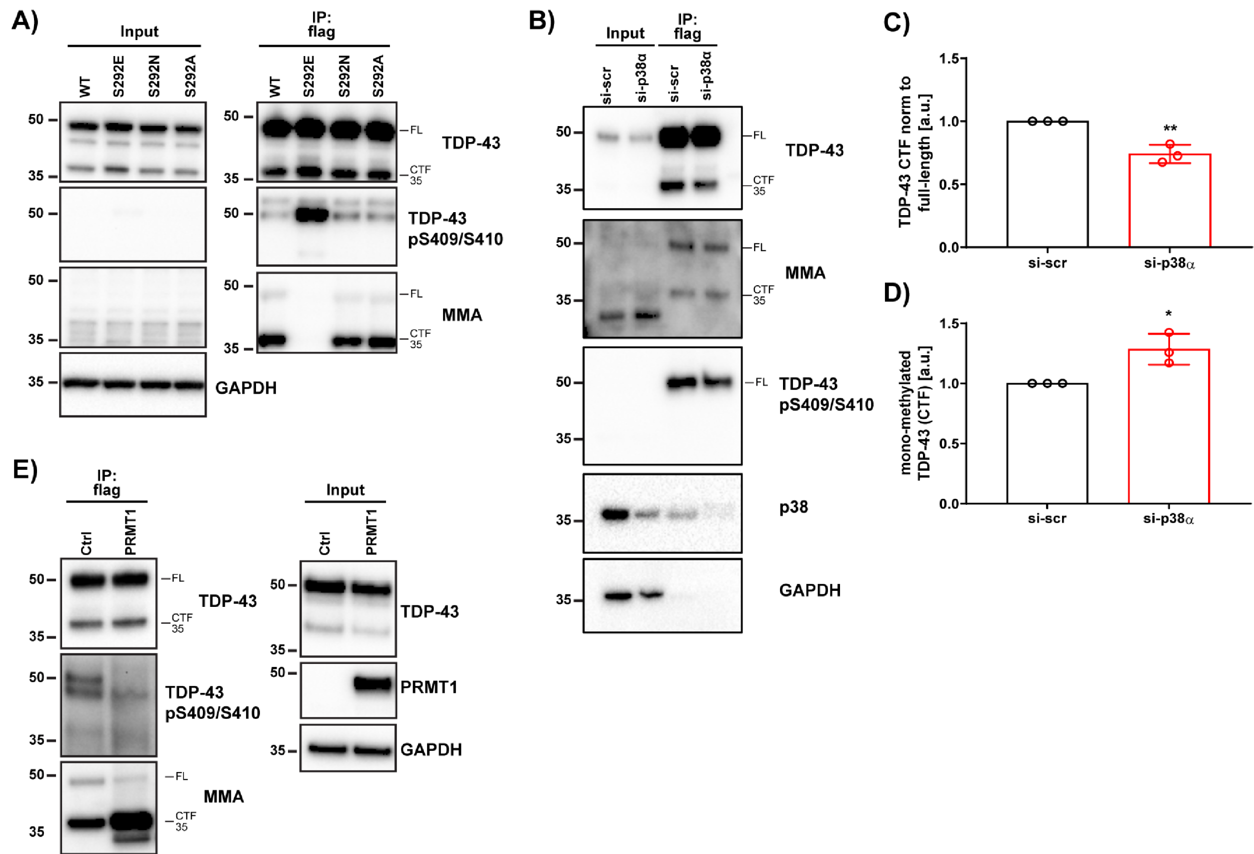

1157

1158 **Figure 7. Crosstalk between PRMT1-catalyzed arginine methylation and p38α-mediated**
1159 **phosphorylation of TDP-43. A)** Western blot of immunoprecipitated flag-tagged TDP-43 from SH-
1160 SY5Y cells probed with antibodies against TDP-43, pTDP-43 and MMA. GAPDH serves as a loading
1161 control. **B)** Western blot of immunoprecipitated flag-tagged TDP-43^{WT} from the SH-SY5Y cells with
1162 and without siRNA-induced p38α knockdown probed with antibodies against TDP-43, p38α, pTDP-
1163 43 and MMA. GAPDH serves as a loading control. **C)** Quantification of TDP-43-CTF/full length-
1164 ratio (mean band signal ± SD, unpaired t test, n = 3). (*p < 0.05, **p < 0.01). **D)** Quantification of
1165 mono-methylated TDP-43-CTF normalized to total TDP-43-CTF (mean band signal ± SD, unpaired
1166 t test, n = 3). (*p < 0.05, **p < 0.01). **E)** Western blot of immunoprecipitated flag-tagged TDP-43^{WT}
1167 from the SH-SY5Y cells with and without PRMT1 overexpression probed with antibodies against
1168 TDP-43, pTDP-43 and MMA. GAPDH serves as a loading control.
1169

bioRxiv preprint doi: https://doi.org/10.1101/2021.08.04.455154; this version posted August 4, 2021. The copyright holder for this preprint (which was not certified by peer review) is the author/funder. All rights reserved. No reuse allowed without permission.

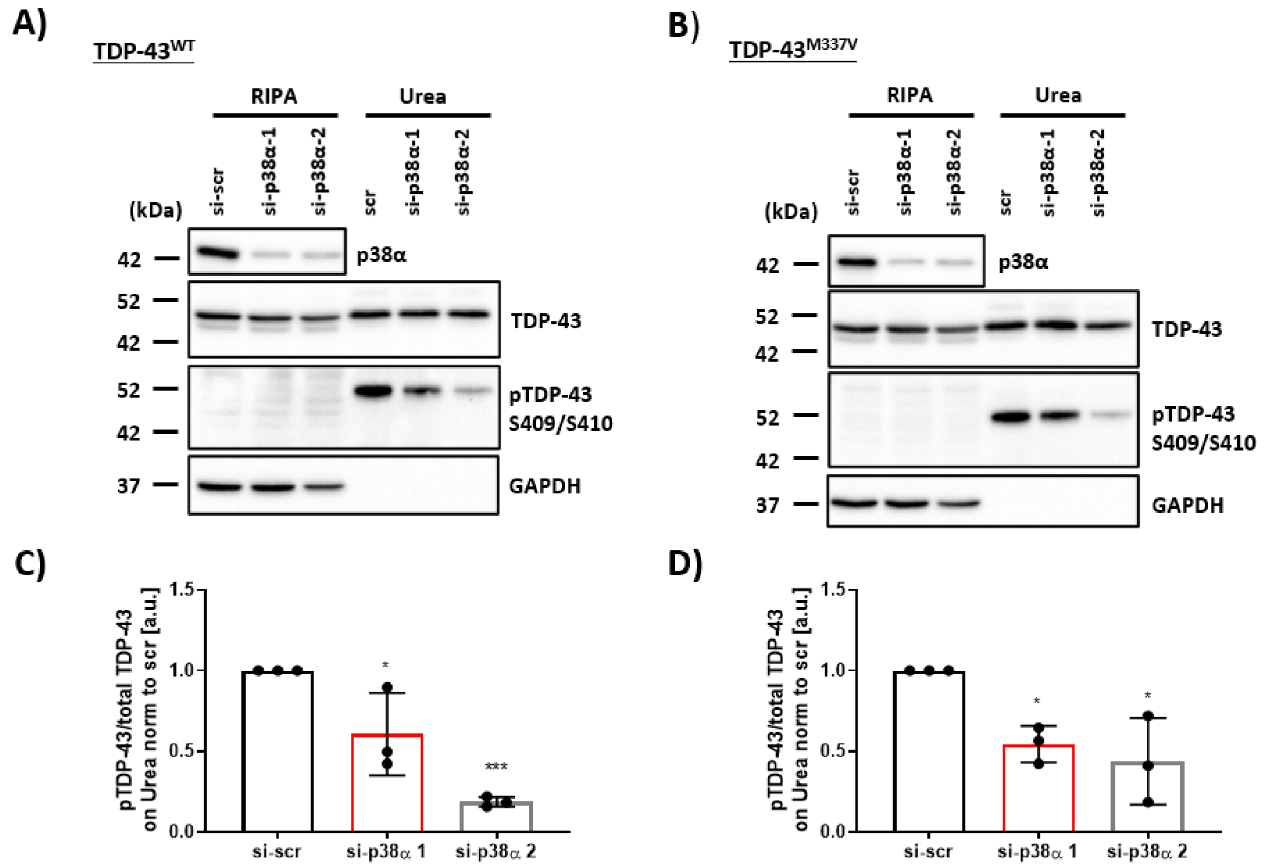

1170

1171 **Figure S1. Genetic ablation of p38α MAPK reduces the aggregation and phosphorylation at**
1172 **S409/S410 for both TDP-43^{WT} and TDP-43^{M337V}. A)** Western blot of total and pTDP-43^{WT} in RIPA
1173 and urea fractions of cells with siRNA-induced p38α knockdown in SH-SY5Y cells after 48h.
1174 GAPDH was used as a loading control. **B)** Western blot of total and pTDP-43^{M337V} in RIPA and urea
1175 fractions of cells with siRNA-induced p38α knockdown in SH-SY5Y cells after 48h. GAPDH was
1176 used as a loading control. **C)** Quantification of pTDP-43^{WT}/total TDP-43^{WT} -ratio in urea fraction
1177 normalized to levels in scrambled siRNA (si-scr). **D)** Quantification of pTDP-43^{M337V}/total TDP-
1178 43^{M337V} -ratio in urea fraction normalized to levels in si-scr (mean band signal ± SD, one-way
1179 ANOVA with Sidak's multiple comparison test, n = 3). $^{*}p < 0.05$, $^{***}p < 0.001$.
1180 Related to Figure 1.
1181

bioRxiv preprint doi: https://doi.org/10.1101/2021.08.04.455154; this version posted August 4, 2021. The copyright holder for this preprint (which was not certified by peer review) is the author/funder. All rights reserved. No reuse allowed without permission.

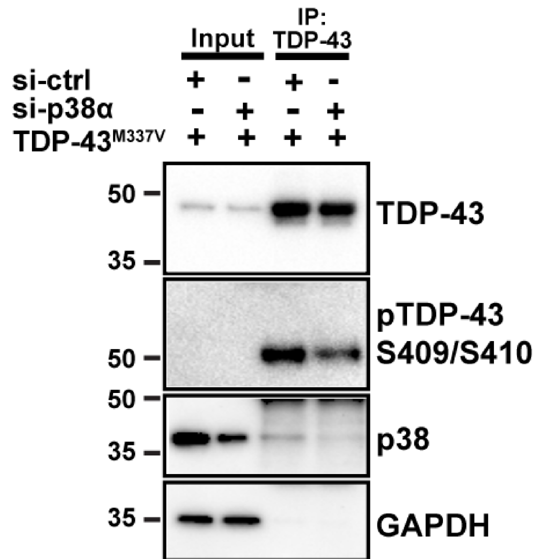

1182

1183 **Figure S2. Knockdown of p38α reduces the co-immunoprecipitation of endogenous p38α with**
1184 **TDP-43.** Western blot of immunoprecipitated TDP-43^{M337V} and co-immunoprecipitated endogenous
1185 p38α from the SH-SY5Y cells with and without siRNA-induced p38α knockdown. GAPDH serves
1186 as a loading control.
1187 Related to Figure 3.
1188
1189